# 4 Damping

## 4.1 Damping Mechanisms and their Mathematical Description

The previous chapter, which dealt with the various types of waves that can occur in a solid body, in all cases made use of some form of Hooke's law that is, it always involved proportionality between stress and strain. Hooke's law, like most laws of physics, is exact only for ideal situations, which represent limiting conditions for practical situations. For the topics treated in the previous chapter, the deviations from Hooke's law exhibited by actual structures are unimportant. However, in relation to processes that, for example, take place over relatively long times one finds that the relations derived in the previous chapter are unsatisfactory. Although it is evident even from cursory observation that every oscillation decays with space and time, the previously derived relations (for example, Eqs. (3.11) and (3.12)) imply that a motion continues forever once it has been started.

The present chapter deals with the aforementioned decay, which is associated with conversion of the energy contained in a given oscillation into a different form of energy. This conversion usually is called damping or dissipation. "Damping" and "dissipation" usually refer only to conversion of mechanical energy into heat. These terms are generally not applied to energy losses that occur as a result of reflection at discontinuities (see Chapter 6), which process is usually described as "attenuation".

Although damping occurs in all types of oscillations, this chapter is concerned only with processes in which mechanical energy is converted into heat. Thus, radiation damping and similar processes are not considered here. The damping of isotropic solids is treated first; then follows a discussion of multilayer systems, for example, plates with damping layers, which are of great practical importance.

Mechanical damping is of interest not only in relation to the control of vibrations and noise, but also for studies of the structure of materials particularly high-polymers and in relation to quality control monitoring.

The question of how the basic equations of elasticity (in the simplest case, Eq. (3.2)) may be modified in order to take into account damping

phenomena has concerned physicists for a long time. As early as 1874, O. E. Meyer [4.1] suggested that a viscous friction force should be taken to act in addition to the elastic forces. Since such a friction force is proportional to the time derivative of the strain, Eq. (3.2) would then be rewritten as the later denoted Kelvin-Voigt model [4.2]

$$\sigma = D\left(\varepsilon + \vartheta \frac{d\varepsilon}{dt}\right). \tag{4.1}$$

For the sinusoidal time variations, which are of greatest interest,

$$\varepsilon = \hat{\varepsilon} \cos \omega t\,, \tag{4.2}$$

is obtained

$$\begin{aligned} \sigma &= D\hat{\varepsilon}\left(\cos\omega t - \omega\vartheta \sin\omega t\right) \\ &= D\hat{\varepsilon}\sqrt{1+\omega^2\vartheta^2}\,\cos\left(\omega t + \arctan\omega\vartheta\right). \end{aligned} \tag{4.3}$$

Thus, for the given periodic strain variation, the stress and strain are not in phase with each other. As will be shown later, this phase difference implies that mechanical energy is transformed into heat in the course of such oscillations.

Equations (4.1) and (4.3) are not quite satisfactory, because it turns out that the parameter $\vartheta$ in reality is strongly frequency dependent. Viscous forces, moreover, within solid bodies are somewhat difficult to imagine. For this reason, Boltzmann [4.3] suggested a different type of relation between stress and strain. He reasoned that the force that produces a given strain does not depend only on that strain, but also on the previous strains i.e., the "strain history". Following Boltzmann and assuming that the effects of the prior strains may be superposed linearly, the dependence of the stress $\sigma(t)$ at time $t$ on the strain $\varepsilon(t)$ at time $t$ and on the strain $\varepsilon(t-\Delta t)$ at the earlier time $(t-\Delta t)$ as can be written as

$$\sigma(t) = D_1\varepsilon(t) - \int_0^\infty \varepsilon(t-\Delta t)\varphi(\Delta t)\,d(\Delta t). \tag{4.4}$$

The function $\varphi(\Delta t)$ describes the "after-effect" of a strain and the form of this function determines the stress-strain relation. One may note that the above reduces to Hooke's law for $\varphi(\Delta t) \equiv 0$, as one would expect.

Of the many "after-effect functions" $\varphi(\Delta t)$ that are possible in principle, only one, the so-called "relaxation function", is physically meaningful. If a strain is imposed on a material, then there occur certain molecular processes (displacements, distortions of crystal lattices, changes in molecular structure, excitation of certain molecular oscillations, etc.), which are ex-

cited gradually, and which then also decay gradually. If the applied strain, for example, causes a molecule chain to oscillate, one may assume that these oscillations will decay exponentially. The corresponding after-effect function then may be written as

$$\varphi(\Delta t) = \frac{D_2}{\tau} e^{-\Delta t/\tau}, \tag{4.5}$$

where $D_2$ is a constant and $\tau$ is the so-called relaxation time, which in the present example is a sort of decay time of molecular oscillations. The form of the stress history for a given strain is shown in Fig. 4.1, for two examples.

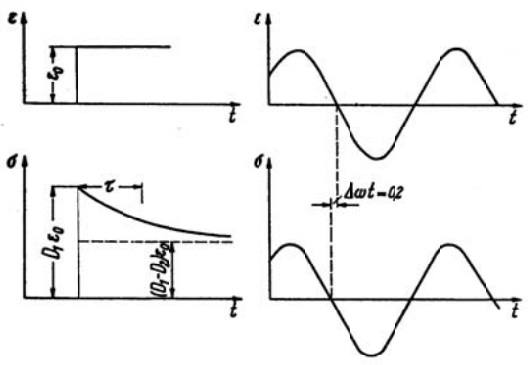


**Fig. 4.1.** Variations of strain and stress with time for a prescribed step-function displacement (left) and sinusoidal displacement (right). Parameters: $D_1 = 2D_2$, $\omega\tau = 0.2$

The left-hand part of the figure indicates the force that is required to produce a step-function jump in the strain from 0 to $\varepsilon_0$. One finds that the initial force is relatively large, but that the force decreases as the body "gets used to" its new state.

The right-hand part of the figure illustrates the stress history for a periodic strain. Because this case is particularly important, it is of interest to analyse it in some detail. Upon introducing Eqs. (4.2) and (4.5) into (4.4), the stress becomes

$$\begin{aligned}\sigma(t) &= D_1\hat{\varepsilon}\cos\omega t - \frac{D_2}{\tau}\hat{\varepsilon}\int_0^\infty \cos\omega(t-\Delta t)e^{-\Delta t/\tau}d(\Delta t)\\ &= \left(D_1 - \frac{D_2}{\omega^2\tau^2+1}\right)\hat{\varepsilon}\cos\omega t - D_2\frac{\omega\tau}{\omega^2\tau^2+1}\hat{\varepsilon}\sin\omega t.\end{aligned} \tag{4.6}$$

Relaxation processes thus lead to a phase shift and therefore to dissipation of mechanical energy. The amount of mechanical energy that is transformed into heat depends on the second term of Eq. (4.6) and thus essentially on the relaxation time and on frequency. For molecular vibrations, these times obviously are very short, but the times $\tau$ corresponding to changes in molecular structure may be very long. Relaxation times may be of the order of hours and days, but also of the order of nanoseconds.

Equations (4.4) and (4.5) permit one to describe all observed stress and strain relations, provided that one accounts for all of the relaxation processes that occur simultaneously i.e., Eq. (4.5) is replaced by a sum of similar expressions with different relaxation times. Therefore, the relaxation model of after-effects may be taken as valid in general.

Unfortunately, the stress-strain relations given so far in Eqs. (4.1) and (4.4) lead to relatively complicated expressions if one tries to use them to derive a wave equation. As is evident from Eqs. (3.9) and (3.10), use of the viscous model of Eq. (4.1) leads to a differential equation of third order, whereas use of the after-effect model of Eq. (4.4) leads even to an integro-differential equation.

Besides the viscous and the relaxation models in (4.1) and (4.4) respectively, there is a number of other suggestions for the mathematical description of damping. Amongst those are the models of Maxwell [4.4] and Zener [4.5] for which the stress-strain relations read

$$\begin{aligned}\frac{d\varepsilon}{dt} &= \frac{1}{D}\frac{d\sigma}{dt} + \frac{1}{\nu}\sigma,\\ \sigma + \tau_1\frac{d\sigma}{dt} &= D\left(\varepsilon + \tau_2\frac{d\varepsilon}{dt}\right),\end{aligned} \tag{4.7}$$

respectively. Herein, $\nu$ denotes the dynamic viscosity while $\tau_1$ and $\tau_2$ are relaxation times. The Maxwell model is primarily used in the description of creep and the Zener model is a combination of that of Eq. (4.1) and the Maxwell model.

## 4.2 Complex Modulus and Wavenumbers

Fortunately, the difficulties associated with the stress-strain relations discussed above can be avoided, if one limits oneself to periodic processes and introduces a complex modulus. As has been pointed out earlier, however, other time dependencies can be handled by means of superposition. Equation (4.3), as well as Eq. (4.6), indicates that the primary effect of damping is the production of a phase difference between stress and strain. One may express this fact very conveniently in complex notation, by writing

$$\sigma(t) = \mathrm{Re}\left\{\underline{D}\hat{\varepsilon}e^{j\omega t}\right\} = D'\hat{\varepsilon}\cos\omega t - D''\hat{\varepsilon}\sin\omega t, \tag{4.8}$$

where

$$\underline{D} = D' + jD'' = D'(1 + j\eta) \tag{4.8a}$$

represents the complex modulus of elasticity. The quantity $\eta = D''/D'$ is the so-called loss factor, which is used widely throughout the rest of this book (in textbooks on polymers often the loss factor is denoted *d*). It should be noted, however, that the complex modulus may lead to causality problems by a transformation from frequency domain to time domain when the loss factor is not known precisely.

**Table 4.1.** Frequency dependence of complex moduli and loss factor

| Type | $D'$ | $D''$ | $\eta$ |
|---|---|---|---|
| Voigt-Kelvin | $D$ | $D\omega\vartheta$ | $\omega\vartheta$ |
| Maxwell | $D\dfrac{\omega^2\nu^2/D^2}{1+\omega^2\nu^2/D^2}$ | $D\dfrac{\omega\nu/D}{1+\omega^2\nu^2D^2}$ | $D/\omega\nu$ |
| Boltzmann | $D_1 - \dfrac{D^2}{1+\omega^2\tau^2}$ | $D_2\dfrac{\omega\tau}{1+\omega^2\tau^2}$ | $\dfrac{D_2\omega\tau}{D_1 - D_2 + D_1\omega^2\tau^2}$ |
| constant loss factor $\eta_0$ | $D$ | $\eta_0 D$ | $\eta_0$ |

In Table 4.1 are shown the real and imaginary parts of the complex Young's modulus as well as the loss factor for the models described above. Figure 4.2a depicts the frequency dependencies and 4.2b the force transmissibility for a single-degree-of-freedom system, containing a spring element incorporating the different damping models. The Zener model is not explicitly included in the table and graphs since it is represented by the Boltzmann model using the substitution $D_2/D_1 = (\tau_2 - \tau_1)/\tau_2$.

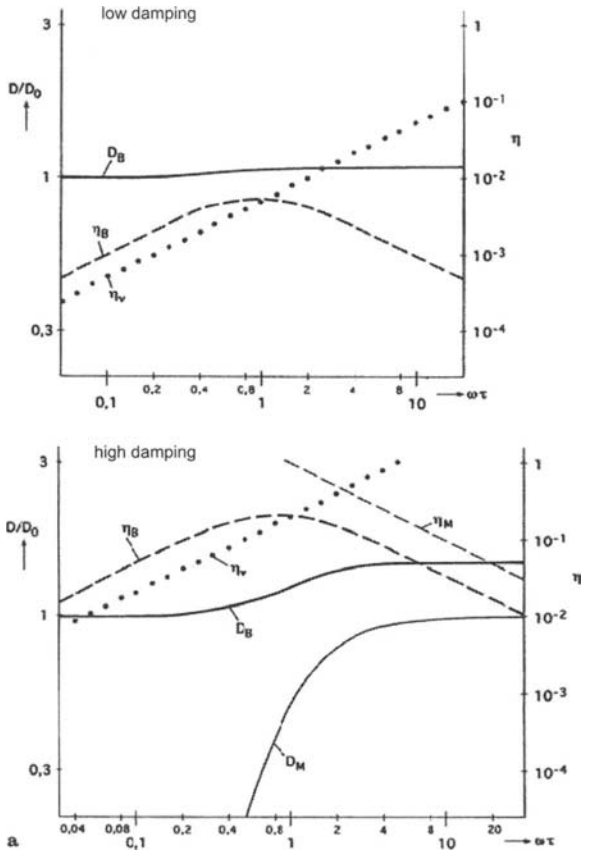


**Fig. 4.2a.** Frequency dependence of the real part of the normalized complex modulus and loss factor. $D_V$, $\eta_V$ – Voigt-Kelvin, $D_B$, $\eta_B$ – Boltzmann and $D_M$, $\eta_M$ – Maxwell

It is seen in Fig. 4.2a that the Boltzmann model increases by a factor of $(1 + \eta_{max})/(1 - \eta_{max})$ in the vicinity of $\omega\tau = 1$ and that there the loss factor is a maximum. For the force transmissibility in Fig. 4.2b it is observed that the Voigt-Kelvin model does not lead to the typical isolation effect that is present at high frequencies for the other models.

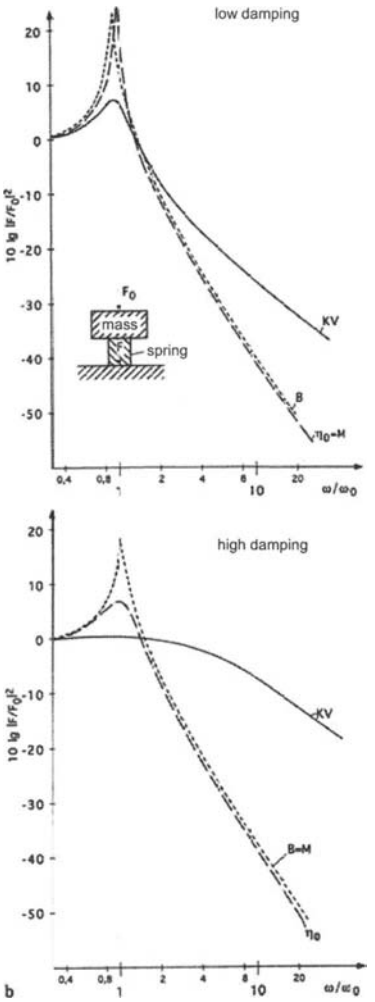


**Fig. 4.2b.** Force transmissibility for a SDOF system. KV – Voigt-Kelvin, B – Boltzmann, M – Maxwell and $\eta_0$ – constant loss factor

If one substitutes the modulus of elasticity $\underline{D}$, as defined above, into the wave equation, one finds that the propagation speed becomes complex. Thus, instead of Eq. (3.13) is obtained

$$\underline{c}_L = c'_L + jc''_L = \sqrt{\frac{\underline{D}}{\rho}} = \sqrt{\frac{\sqrt{D'^2 + D''^2} + D'}{2\rho}} + j\sqrt{\frac{\sqrt{D'^2 + D''^2} - D'}{2\rho}}. \qquad (4.9)$$

For weak damping, that is $D' >> D''$ or $\eta << 1$, one may approximate Eq. (4.9) by

$$\underline{c}_L \approx \sqrt{\frac{D'}{\rho}}\left(1 + j\frac{\eta}{2}\right). \tag{4.9a}$$

Even for $\eta = 0.5$, this approximation deviates from the exact value only by about 4 %. Errors that exceed 10 % result only for $\eta > 1$. The wavenumber also becomes complex, of course, namely,

$$\underline{k}_L = \frac{\omega}{\underline{c}_L} = k_L' - jk_L'' \approx \omega\sqrt{\frac{\rho}{D'}}\left(1 - j\frac{\eta}{2}\right). \tag{4.10}$$

For propagation in the positive $x$-direction, the above expression must be multiplied by –1, for propagation in the negative $x$-direction, by +1.

Similar expressions hold also for quasi-longitudinal waves on plates and beams, as well as for torsional and transverse waves. An additional simplification occurs for homogeneous isotropic materials, because the loss factors associated with extension and shear of such materials generally are found to be equal. (For anisotropic solids, this is generally not the case.) For transverse waves, in the presence of weak damping, one finds

$$\underline{c}_T \approx \sqrt{\frac{G'}{\rho}}\left(1 + j\frac{\eta}{2}\right); \quad \underline{k}_T \approx \pm\omega\sqrt{\frac{\rho}{G'}}\left(1 - j\frac{\eta}{2}\right). \tag{4.11}$$

For pure bending waves, introduction of the appropriate complex modulus into Eq. (3.85) yields

$$\underline{c}_B \approx \sqrt[4]{\omega^2\frac{B'}{m'}}\left(1 + j\frac{\eta}{4}\right) \tag{4.12a}$$

and the corresponding wavenumber

$$\underline{k}_B \approx \sqrt[4]{\omega^2\frac{m'}{B'}}\left(1 - j\frac{\eta}{4}\right). \tag{4.12b}$$

The physical meaning of a complex wavenumber (or of a complex propagation speed) becomes evident at once if one introduces it into the appropriate phasor relation. For plane waves propagating in the positive $x$-direction, which may be described by

$$u(x,t) = \mathrm{Re}\left\{\hat{u}e^{j\omega t - jkx}\right\} = \hat{u}\cos(\omega t - kx + \varphi), \tag{4.13}$$

use of the complex wavenumber results in

$$u(x,t) = \mathrm{Re}\left\{\hat{u}e^{j\omega t - jk'x - k''x}\right\} = \hat{u}e^{-k''x}\cos(\omega t - k'x + \varphi). \tag{4.14}$$

A complex wavenumber – that is, a complex modulus – thus implies exponential decay of propagating plane waves.

For lightly damped longitudinal, transverse and torsional waves $k'' = k'\eta/2 = \pi\eta/\lambda$ . Thus, Eq. (4.14) implies that the amplitude decays by a factor of $e^{-\pi\eta}$ within a wavelength. Within a distance $\Delta x$ there therefore occurs a reduction in level by

$$\Delta L = \frac{8.7\pi\eta\Delta x}{\lambda}\,\mathrm{dB}. \tag{4.15}$$

A different expression holds for bending waves, because for these $k_B'' \approx \pi\eta/2\lambda_B$ . Here the decrease in level with distance obeys

$$\Delta L_B = \frac{4.34\pi\eta\Delta x}{\lambda_B}\,\mathrm{dB}. \tag{4.16}$$

The reason that Eqs. (4.15) and (4.16) differ by a factor of 2 is that for bending waves the group speed, which determines the energy propagation, and thus also the damping is twice the phase velocity, see Eq. (3.89).

A difficulty arises, however, in relation to the nearfields of flexural waves. Namely, if Eq. (4.12b) is used to determine the nearfield wavenumber (see Eq. (3.109)), then there result nearfields of the form

$$e^{k_B'x - jk_B''x}, \quad e^{-k_B'x + jk_B''x}.$$

One obtains so-called complex nearfields, for which the amplitude decrease occurs in the direction which is opposite to propagation direction. At first glance, this result appears to have little physical meaning, because it appears to lead to increasing amplitudes. However, Tamm and Weis [4.6, 4.7] have shown that such complex nearfields occur very often at the higher-modal vibrations of plates, see Sect. 3.7. By considering the two related conjugate complex wavenumbers as corresponding to a decaying standing wave, one may remove the apparent violation of the law of conservation of energy. For the remainder of this discussion, however, complex nearfields are of relatively little interest.

For the more complicated vibrations that were treated in Sect. 3.7 (particularly in Fig. 3.25), one may also obtain the propagation speeds and damping by introduction of complex moduli. The corresponding equations, however, turn out to be very complicated. At present, solutions are available only for rubber-elastic plates ($\mu = 0.5$) with pure shear losses [4.7]. The analysis shows that with large losses the modes associated with high propagation speeds ($c >> c_T$) are damped very strongly, so that in essence

there only remain bending or Rayleigh waves, transverse waves, and quasi-longitudinal waves.

Not only the spatial variations associated with a vibration are of interest, but also the corresponding energy relations. Consider a system that is excited so as to oscillate at a angular frequency ω, for example, a rod excited longitudinally by means of an electrodynamic shaker. The strains that occur in a given elementary volume of such a system may again be written as

$$\varepsilon(t) = \mathrm{Re}\left\{\hat{\varepsilon} e^{j\omega t}\right\} = \hat{\varepsilon}\cos(\omega t + \varphi). \tag{4.17}$$

The corresponding stresses then obey

$$\begin{aligned}\sigma &= \mathrm{Re}\left\{\underline{D}\hat{\varepsilon} e^{j\omega t}\right\} = \hat{\varepsilon} D'\cos(\omega t + \varphi) - \hat{\varepsilon} D''\sin(\omega t + \varphi) \\ &= \hat{\varepsilon} D'\sqrt{1+\eta^2}\,\cos(\omega t + \arctan\eta + \varphi),\end{aligned} \tag{4.18}$$

see Eqs. (4.3), (4.6) and (4.8). One may note that the phase difference between stress and strain is directly related to the loss factor η. If one determines the potential energy density according to Eq. (3.6), then one obtains

$$\begin{aligned}E_{pot} &= \int_0^{\varepsilon} \sigma\, d\varepsilon \\ &= \frac{\hat{\varepsilon}^2 D'}{2}\left[\eta\omega t + \frac{\sqrt{1+\eta^2}}{2}\cos(2\omega t + \arctan\eta + 2\varphi) + \mathrm{const}\right].\end{aligned} \tag{4.19}$$

In this equation "const" represents a constant the depends on the limits of the integration and that is unimportant here. The variation of energy density with time given by Eq. (4.19) is plotted in Fig. 4.3.

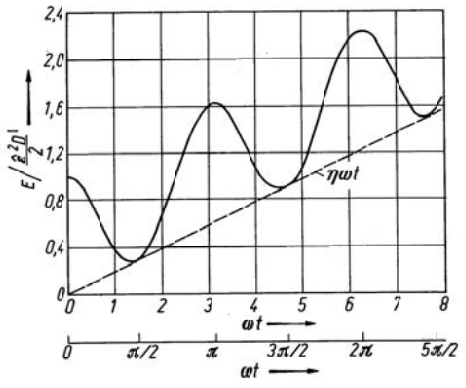


**Fig. 4.3.** Time-dependence of potential energy in a sinusoidally vibrating damped material. Calculated from Eq. (4.19) for η = 0.2

As evident from this figure, the average energy density increases with time. Because the amplitude of the vibration and thus the mechanical (reversible) energy remains constant, however, the additional energy supplied to the system which corresponds to the term $\eta\omega t$ in Eq. (4.19) evidently must be transformed into another form of energy (heat). The energy that the shaker continuously feeds into the sample in the last analysis serves to heat the material.

A stress-strain diagram is useful for providing further insight. If one introduces Eq. (4.17) into (4.18), one obtains

$$\sigma^2 - 2\sigma\varepsilon D' + \varepsilon^2 D'^2 \left(1+\eta^2\right) = \eta^2 D'^2 \hat{\varepsilon}^2. \tag{4.20}$$

This equation represents an ellipse, centred at the origin, as shown non-dimensionalized in Fig. 4.4. Indicated are also the lengths of the semi-axis. The elliptical area is

$$S_E = \pi\sqrt{2}\,\frac{\eta}{\sqrt{2}} = \pi\eta.$$

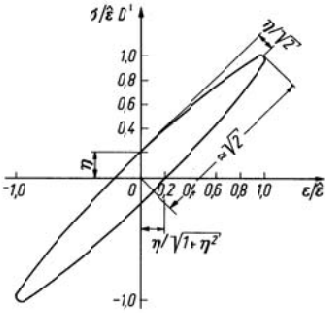


**Fig. 4.4.** Stress-strain curve of a dissipative material under sinusoidal loading ($\eta = 0.2$)

Since the energy $E_l$ lost during one cycle of a vibration with period $T$ is given by

$$E_l = \oint \sigma\, d\varepsilon = D'\hat{\varepsilon}^2 \oint \left(\frac{\sigma}{D'\hat{\varepsilon}}\right) d\left(\frac{\varepsilon}{\hat{\varepsilon}}\right) = D'\hat{\varepsilon}^2 S_E,$$

which corresponds precisely to the area of the ellipse, one finds that

$$E_{diss} = \pi\eta D'\hat{\varepsilon}^2. \tag{4.21}$$

The energy lost in a time interval $t$ thus is given by $E_{diss}t/T = E_{diss}\omega t/2\pi = \hat{\varepsilon}^2 D'\eta\omega t/2$. This result corresponds exactly to the time-average value obtained from Eq. (4.19).

From these energy relations can be developed a convenient and physically meaningful definition of the loss factor. If one divides Eq. (4.21) by the (reversible) mechanical energy $E_R = D'\hat{\varepsilon}^2/2$, one obtains

$$\eta = \frac{E_l}{2\pi E_R}. \tag{4.22}$$

Thus, the loss factor indicates what fraction of the vibratory (reversible) mechanical energy is lost (i.e., converted into heat) in one cycle of the vibration. Note that the reversible energy appears in the denominator of Eq. (4.22), and not the total energy, which is usually used in definitions of efficiency. This distinction, however, is unimportant for small damping. The relation between the reversible energy and the periodically varying total energy is evident from Fig. 4.3.

In practice one is interested not only in the energy loss which occurs in a system whose vibration amplitude is kept constant by continuous external excitations, but one is also concerned with the time-wise decay of vibrations that results when the excitation is removed, so that energy is no longer supplied to the system. The over a period dissipated energy is obtained from the definition in (4.22), $E_{diss} = 2\pi\eta\ E_R$ such that the time dependence becomes

$$E_{diss}(t) = E_{diss}\frac{t}{T} = \omega\eta E_R t. \tag{4.22a}$$

Consider a system that vibrates at the angular frequency ω and which at time $t = 0$ has a reversible mechanical energy $E_{R0}$. If the system is disconnected at time $t = 0$ from all external sources, then all of its mechanical energy $E_{R0}$ will eventually be converted into heat. In order to simplify the analysis, it is convenient to assume that the system under consideration has only one energy storage mechanism. Thus, for example, cases where energy can be stored in coupled bending waves and torsional waves are excluded here. Further, it is useful to postulate that the change in the amplitude (peak value) that occurs in one period of the oscillation is small. If the energy that is changed into heat up to time $t$ is denoted by $E_{diss}(t)$, then the reversible energy that is left in the system at this time is $E_R\ (t) = E_{R0} - E_{diss}(t)$, in view of conservation of energy. The energy converted into heat during the time interval between $t$ and $t + dt$ thus is $[E_{R0} - E_{diss}(t)]\ \eta\omega\ dt$, in view of the first term of Eq. (4.19). The total energy converted into heat up to time $t$ is obtained by adding the losses for all earlier times,

$$E_{diss}(t) = \int_0^t \left[ E_{R0} - E_l(t) \right] \eta\omega \, dt. \tag{4.23}$$

If one differentiates Eq. (4.23) with respect to $t$, one obtains a simple differential equation for $E_{diss}(t)$, which has exponential solutions, as would be expected,

$$E_{diss}(t) = E_{R0}\left(1 - e^{-\eta\omega t}\right) \quad \text{or} \quad E_R(t) = E_{R0} e^{-\eta\omega t}. \tag{4.24}$$

The energy thus decays exponentially, with a decay constant $\eta\omega$.

## 4.3. Resonant Vibrations of Damped Beams

One procedure that is often used for experimental determination of the loss factor involves measuring the response amplitude of a system as a function of frequency, for a constant excitation amplitude, and deducing the loss factor from the so-called bandwidth of response peaks – the half-power bandwidth. This method is well-known for measurement of the damping of systems with one degree of freedom and it is treated here in some detail, because in measurements on beams and similar structures there arise some considerations which one does not encounter for single-degree-of-freedom systems. The conversion from one damping quantity to another is facilitated by Table 4.2.

**Table 4.2.** Conversion formulae for damping quantities

| Loss factor $\eta$ = | $\eta$ | $b/f$ | $2.2/Tf$ | $\Lambda/\pi$ |
|---|---|---|---|---|
| Bandwidth (Hz) $b$ = | $\eta f$ | $b$ | $2.2/T$ | $\Lambda f/\pi$ |
| Reverberation time (sec) $T$ = | $2.2/\eta f$ | $2.2/b$ | $T$ | $6.8/\Lambda f$ |
| Logarithmic decrement $\Lambda$ = | $\eta\pi$ | $\pi b/f$ | $6.8/Tf$ | $\Lambda$ |
| Phase angle (rad) $\varphi$ = | arctan $\eta$ | arctan $(b/f)$ | arctan $(2.2/Tf)$ | arctan $(\Lambda/\pi\varphi)$ |

$\lambda$ = wavelength (m); $c$ = phase speed (m/sec)

Additional relations:

$\underline{k}_L \approx k'_L \ (1 - j\eta/2)$ for longitudinal waves

$\underline{k}_B \approx k'_B \ (1 - j\eta/4)$ for bending waves

Level decay for plane bending waves: $D'_B = 13.6\ \eta/\lambda$ [dB/m]

Level decay for longitudinal waves: $D'_L = 27.2\ \eta/\lambda$ [dB/m]

$\underline{E} = E' \ (1 + j\eta)$

### 4.3.1 Quasi-Longitudinal Waves and Torsional Waves

Of the many methods available for the analysis of beam vibrations, the one used in this section – which deduces the vibrations of a finite beam from the behaviour of an infinite one – may be somewhat cumbersome, but provides considerable physical insight. Consider a rod, such as that shown in Fig. 4.5, excited at one end by the force

$$F = \mathrm{Re}\left\{\underline{\hat{F}} e^{j\omega t}\right\}.$$

In an infinitely long rod, such an excitation would give rise to a wave motion

$$\underline{\hat{v}}_0(x) = \frac{\hat{F}}{\underline{Z}} e^{-j\underline{k}x}, \tag{4.25}$$

where $\underline{Z}$ represents the complex driving-point impedance (which takes on a complex value, because the propagation speed is complex), and $\underline{k}$ is the complex wavenumber. For quasi-longitudinal waves, the driving-point impedance at a free end is $S\rho\,\underline{c}_{L\mathrm{II}}$.

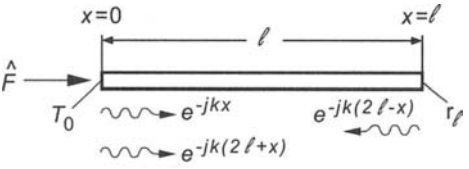


**Fig. 4.5.** Wave propagation along a beam

When the wave given by Eq. (4.25) arrives at the end of the rod, the velocity amplitude is

$$\frac{\hat{F}}{\underline{Z}} e^{-j\underline{k}l}.$$

The wave now is reflected, resulting in a backward travelling wave given by

$$\frac{\hat{F}}{\underline{Z}} \underline{r}_l e^{-j\underline{k}(2l-x)},$$

where $\underline{r}_l$ represents the (complex) reflection coefficient at the location $x = l$. This wave is reflected once again when it reaches $x = 0$, and the doubly reflected wave obeys

$$\frac{\hat{F}}{\underline{Z}} \underline{r}_l \underline{r}_0 e^{-j\underline{k}(2l+x)},$$

where $\underline{r}_0$ denotes the reflection coefficient at $x = 0$. This doubly reflected wave is again reflected at $x = l$, and this process is repeated again and again, indefinitely. In the steady state, where all these components are present simultaneously, one thus obtains

$$\underline{v}(x) = \frac{F}{\underline{Z}}\left[ e^{-j\underline{k}x} + \underline{r}_l e^{-j\underline{k}(2l-x)} + \underline{r}_0 \underline{r}_l e^{-j\underline{k}(2l+x)} + \underline{r}_0 \underline{r}_l^2 e^{-j\underline{k}(4l-x)} \ldots \right]. \tag{4.26}$$

One may note that the first, third, fifth, … terms of this expression form a geometric series with the ratio $\underline{r}_0\underline{r}_l e^{-2j\underline{k}l}$ and the same holds also for the second, fourth, sixth, … terms. Thus, by applying the summation formula for infinite geometric series, one obtains

$$\underline{v}(x) = \frac{F}{\underline{Z}} \frac{e^{-j\underline{k}x} + \underline{r}_l e^{-j\underline{k}(2l-x)}}{1 - \underline{r}_0 \underline{r}_l e^{-2j\underline{k}l}}. \tag{4.27}$$

Equation (4.27) also illustrates once again that the resonances i.e., the zeros or the minima of the denominator, correspond to the principle of wave-train closure, see Sect. 3.4. Closure of a wave train on itself here involves precisely a phase shift by $2\underline{k}l$ and reflection at both ends of the rod; one thus obtains wave train closure if $\underline{r}_0\underline{r}_l e^{-2j\underline{k}l}$ is as close to unity as possible.

It is of interest to consider several limiting cases, in order to illustrate the general validity of Eq. (4.27). For a rod that is free at both ends ($\underline{r}_0 = \underline{r}_l = 1$) and very short ($\underline{k}l << 1$), one may approximate the exponential term of Eq. (4.27) by the first element of its series expansion

$$\underline{v}(x) \approx \frac{F}{\underline{Z}} \frac{1}{j\underline{k}l}. \tag{4.28}$$

For quasi-longitudinal waves, $\underline{Z}\ \underline{k}l = \omega\rho Sl$, and the above result implies that a short rod which is free at both ends behaves essentially as a mass, as one would expect.

For a rod that is free at one end and clamped at the other ($\underline{r}_0 = 1$, $\underline{r}_l = -1$), one finds by multiplying Eq. (4.27) by $e^{jkl}$ that

$$\underline{v}(x) = j \frac{F}{\underline{Z}} \frac{\sin \underline{k}(l-x)}{\cos \underline{k}(l-x)}. \tag{4.29}$$

In the special case of short rods ($\underline{k}l << 1$) the velocity at $x = 0$ obeys

$$\underline{v}(0) \approx j\underline{k}l\frac{F}{\underline{Z}}; \tag{4.30}$$

and for quasi-longitudinal waves, for which $\underline{Z} = S\sqrt{\underline{E}\rho}$ and $k = \omega\sqrt{\rho / \underline{E}}$,

$$\underline{v}(0) \approx j\frac{\omega lF}{S\underline{E}}; \tag{4.31}$$

thus, such short rods behave like pure springs.

The behaviour of Eq. (4.27) in the vicinity of minima of the denominator is of particular importance in relation to measurements. In order to find these minima, one may assume that at the two ends of the rod there occur no energy losses i.e. $|r| = 1$, but only the phase shifts $\gamma_0$ and $\gamma_l$ respectively, see Sect. 3.4. If one introduces the complex wavenumber $\underline{k} = k' - jk''$ as defined in Eq. (4.10), then one may rewrite the denominator of Eq. (4.27) as

$$1 - e^{-2k''l}\left[\cos\left(2k'l - \gamma_0 - \gamma_l\right) - j\sin\left(2k'l - \gamma_0 - \gamma_l\right)\right]. \tag{4.32}$$

With small damping that is, for $k''l << 1$, this function takes on its minimum value i.e., the velocity reaches its maximum for

$$2k'l - \gamma_0 - \gamma_l = 2n\pi.$$

By comparing this result with Eq. (3.106), one finds that it corresponds precisely to the resonance frequencies of undamped rods. If the damping is not small, one must find the minima of Eq. (4.32) by setting the derivative of the equation with respect to $k'$ equal to zero. These resonance frequencies turn out to be somewhat lower than those of similar lightly damped rods.

Whether the minima of the denominator of Eq. (4.27) correspond to maxima of the velocity also depends on the observation point. The numerator of Eq. (4.27) is periodic in $x$, that is, there occur nodes and antinodes of vibration. This is illustrated in Fig. 4.6a, which shows the frequency dependence of the velocity for various amounts of damping, and in Fig. 4.6b, which shows the spatial dependence of the velocity. Both these figures pertain to a rod that is free at both ends and excited by a force of constant (frequency independent) amplitude. The corresponding velocity obeys

$$\left|\underline{v}(x)\right|^2 = \left|\frac{F}{\underline{Z}}\right|^2 \frac{\cosh 2k''(l-x) + \cos 2k'(l-x)}{\cosh 2k''l - \cos 2k''l}. \tag{4.33}$$

The abscissa of Fig. 4.6a is $k'l$ (the wavenumber, multiplied by the beam length) and thus is proportional to the frequency, and the abscissa of Fig. 4.6b is $k'x$. The ordinate of these figures is the logarithm of the ratio of the velocity to an arbitrary reference velocity $v_0$. One may note that the curves become flatter with increasing frequency, and eventually behave like exponentially decaying functions. For $k''/k' = 0.5$, that is for $\eta \approx 1$, the curves would exhibit no recognizable periodicity at all.

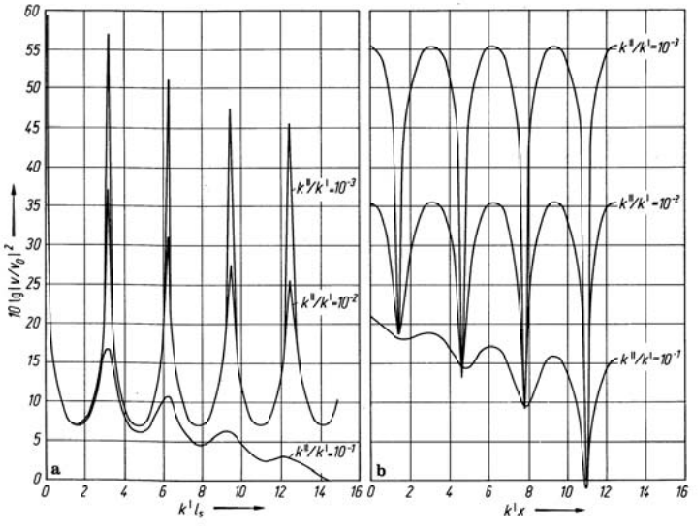


**Fig. 4.6.** Quasi-longitudinal or torsional vibrations of free-free beams, as determined from Eq. (33). a) Variation with frequency at $x = l$; b) Variation with position, for $k^{\perp}l = 4\pi$

For small damping, one may obtain simplified expressions for the behaviour in the vicinity of resonances by developing Eq. (4.27) in a series about a resonance condition. In this development, however, one must take into account that both the numerator and the denominator depend on frequency. Assume that the velocity is measured at an anti-node i.e., a maximum in Fig. 4.6b, thus, at a position where the curve corresponding to the spatial variation is very flat and thus unaffected by small changes in $k'x$. Because of this assumption, the analysis that follows is not valid for nodal positions, since there small changes in frequency lead to large changes in the numerator and denominator of Eq. (4.27). For the anti-nodes it is found that

$$\underline{v}_B = \frac{\underline{v}_0}{1-\left|\underline{r}_0\underline{r}_l\right| e^{-2k''l} e^{-j\left(2k'l-\gamma_0-\gamma_l\right)}}.$$

If the damping is small, and only the behaviour in the vicinity of resonances is of interest, then one may use the approximations $e^{-2k''l} \approx 1-2k''l = 1-2\eta k'l$ and $e^{-j\left(2k'l-\gamma_0-\gamma_l\right)} \approx 1-2\Delta k'l$, and write

$$\underline{v}_B \approx \frac{\underline{v}}{1-\left|\underline{r}_0\underline{r}_l\right|\left(1-2k''l-2j\Delta k'l\right)}.$$

Since this expression has its maximum value $v_{\max}$ at resonance ($\Delta k'l = 0$),

$$\frac{\underline{v}_B}{\underline{v}_{\max}} \approx \frac{1-\left|\underline{r}_0\underline{r}_l\right|\left(1-2k''l\right)}{1-\left|\underline{r}_0\underline{r}_l\right|\left(1-2k''l-2j\Delta k'l\right)} = \frac{1}{1+j\dfrac{\Delta k'l}{k''l+\left(1-\left|\underline{r}_0\underline{r}_l\right|\right)/2\left|\underline{r}_0\underline{r}_l\right|}},$$

from which it is found

$$\left|\frac{\underline{v}_B}{\underline{v}_{\max}}\right|^2 \approx \frac{1}{1+\left[\dfrac{\Delta k'}{k'}\dfrac{1}{\left(k''/k'\right)+\left(1-\left|\underline{r}_0\underline{r}_l\right|\right)/2\left|\underline{r}_0\underline{r}_l\right|k'l}\right]^2}. \tag{4.34}$$

In the vicinity of the resonance frequency, a plot of $\underline{v}_B$ versus frequency thus has the typical resonance response character, see Fig. 4.7. The width of the resonance curve here depends on the energy losses due to reflection and internal damping. If no energy losses are due to reflections ($|\underline{r}_0\underline{r}_l| = 1$), then Eq. (4.34) reduces to

$$\left|\frac{\underline{v}_B}{\underline{v}_{\max}}\right|^2 \approx \frac{1}{1+\left(\dfrac{\Delta k'}{k''}\right)^2}. \tag{4.35}$$

If the wavenumbers are expressed in terms of the frequency to which they are proportional, then $\Delta k'/k'$ becomes $\Delta f/f_n$, where $\Delta f$ represents the frequency deviation measured from the peak frequency $f_n$. If one also sets $k'' = \eta k'/2$ (see Eq. (4.10)), one obtains

$$\left|\frac{\underline{v}_B}{\underline{v}_{\max}}\right|^2 \approx \frac{1}{1+\left(\dfrac{2\Delta f}{\eta f_n}\right)^2}. \tag{4.36}$$

The half-value bandwidth of the resonance curve, thus, is $b = \eta f_n$, see Fig. 4.7. Clearly, measurement of this resonant behaviour constitutes a simple

means for determining the damping, provided that the loss factor is not too great and the measurements are carried out at an anti-node.

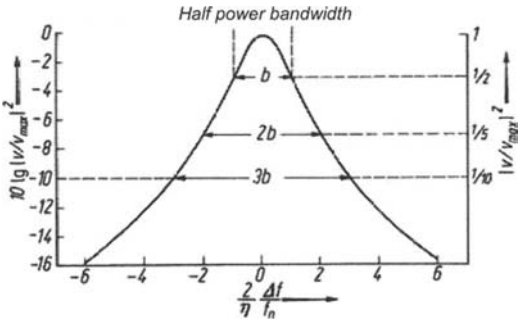


**Fig. 4.7.** Vibrational response of lightly damped systems in the vicinity of a resonance

For the vibrations in the vicinity of nodes, one finds that at constant frequency,

$$\left|\underline{v}_K\right|^2 \approx \left|\underline{v}_{\min}\right|^2 \left[1+\frac{4\left|\underline{r}_l\right| e^{-2k''(l-x)}}{\left(1-\left|\underline{r}_l\right| e^{-2k''(l-x)}\right)^2}\left(k\Delta x\right)^2\right]. \tag{4.37}$$

for vanishingly small damping ( $k'' = 0$), this reduces (for $\underline{r}_l \approx 1$) to

$$\left|\underline{v}_K\right|^2 \approx \left|\underline{v}_{\min}\right|^2 \left[1+\left(\frac{2k\Delta x}{1-\left|\underline{r}_l\right|}\right)^2\right] = \left|\underline{v}_{\min}\right|^2 \left[1+\left(\frac{4\pi}{1-\left|\underline{r}_l\right|}\right)^2\left(\frac{\Delta x}{\lambda}\right)^2\right]. \tag{4.38}$$

For complete reflection at the end ($|\underline{r}_l| = 1$), the approximation $e^{-2k''(l-x)} = 1-2k''\left(l-x\right)$ may be used to obtain

$$\left|\underline{v}_K\right|^2 \approx \left|\underline{v}_{\min}\right|^2 \left[1+\left(\frac{\Delta x}{l-x_n}\right)^2\frac{k'^2}{k''^2}\right]. \tag{4.39}$$

As can be observed, there exists a close relation between the vibrations near a resonance and near a node. The resonance frequency $f_n$ is analogous to the location $x_n$ of a node, and the frequency interval $\Delta f$ is analogous to the distance $\Delta x$. The fact that the expression 1 + … occurs in the numerator

in one case and in the denominator in the other makes little difference, particularly if the velocity is represented logarithmically.

There are available many methods for analysing the vibrations of a rod, in addition to that used above. Among the most important of these is the so-called "four-pole" representation. This representation can be developed by considering the wave field in a rod to be composed of forward and backward propagating waves, for which the velocity may be expressed as

$$\underline{v}(x) = \underline{v}_+ e^{-j\underline{k}x} + \underline{v}_- e^{j\underline{k}x}, \tag{4.40}$$

where $v_+$ and $v_-$ are unknown for the present. The corresponding force that acts in the beam is given by

$$\underline{F}(x) = \underline{Z}\underline{v}_+ e^{-j\underline{k}x} - \underline{Z}\underline{v}_- e^{j\underline{k}x} \tag{4.40a}$$

where the change in the algebraic sign results from the different directions of wave propagation. The above must hold for all locations, and thus also for $x = 0$. One therefore obtains the following conditions for $v_+$ and $v_-$:

$$\underline{v}_0 = \underline{v}_+ + \underline{v}_-, \quad \underline{F}_0 = \underline{Z}(\underline{v}_+ - \underline{v}_-).$$

If one introduces the resulting values of $v_+$ and $v_-$ into Eqs. (4.40) and (4.40a), then one obtains that at the location $x = l$, for example

$$\begin{aligned} \underline{v}_l &= \underline{v}_0 \cos \underline{k}l - j\frac{\underline{F}_0}{\underline{Z}} \sin \underline{k}l \\ \underline{F}_l &= -j\underline{Z}\underline{v}_0 \sin \underline{k}l + \underline{F}_0 \cos \underline{k}l. \end{aligned} \tag{4.41}$$

Equations (4.41) are a four-pole representation of the rod. They relate the velocity and the force at its beginning to the velocity and force at its end. Inversion of Eqs. (4.41) gives

$$\begin{aligned} \underline{v}_0 &= \underline{v}_l \cos \underline{k}l + j\frac{\underline{F}_l}{\underline{Z}} \sin \underline{k}l \\ \underline{F}_0 &= j\underline{Z}\underline{v}_l \sin \underline{k}l + \underline{F}_l \cos \underline{k}l. \end{aligned} \tag{4.41a}$$

Of course, Eqs. (4.41a) and (4.27) always lead to the same result.

It depends on the particular problem to be solved whether Eq. (4.27) or the four-pole representation of Eq. (4.41a) is more advantageous for the analysis. Equation (4.27) is preferable if the reflection coefficients are known. If one is concerned with the transmission from one arbitrary system via the rod to another system, however, then the four-pole representation generally is more convenient.

### 4.3.2 Bending Waves

In order to apply the previously used analysis procedure for bending waves, one needs to replace the simple exponential functions in Eqs. (4.25) to (4.27) by the more complicated propagation functions for bending waves, which consist of nearfields and propagating waves. Because the associated manipulations are cumbersome and lengthy, it is useful to investigate bending waves on beams by means of a different approach. Equation (4.27) also gives a good approximation for bending waves on beams that are not too short, provided that the correct reflection coefficients are used. (For example, for a free-free beam, $\underline{r}_0 = \underline{r}_l = -j$.) This approximation only involves neglecting the nearfields; therefore the results derived in the previous section also apply to bending waves, for locations farther than a half wavelength from the beam ends.

As evident from Eq. (3.109), beam bending vibrations involve four component solutions:

$$\underline{v} = \underline{v}_+ e^{-j\underline{k}x} + \underline{v}_- e^{j\underline{k}x} + \underline{v}_{-j} e^{-\underline{k}x} + \underline{v}_{+j} e^{\underline{k}x}. \tag{4.42}$$

One may use this equation, or the equivalent expression

$$\underline{v} = \underline{v}_1 \cosh \underline{k}x + \underline{v}_2 \sinh \underline{k}x + \underline{v}_3 \cos \underline{k}x + \underline{v}_4 \sin \underline{k}x, \tag{4.42a}$$

depending on which of the two leads to simpler manipulations. The four unknowns $\underline{v}_+$, $\underline{v}_-$, $\underline{v}_{+j}$, $\underline{v}_{-j}$, or $\underline{v}_1$, $\underline{v}_2$, $\underline{v}_3$, $\underline{v}_4$, respectively may be evaluated from the four boundary conditions. For example, for a free-free beam that is excited by a force $F_0$ at $x = 0$, see Sect. 3.4.2, one obtains

$$\begin{aligned}
\underline{M}(l) &\equiv -\frac{B\underline{k}^2}{j\omega}\left[-\underline{v}_+ e^{-j\underline{k}l} - \underline{v}_- e^{j\underline{k}l} + \underline{v}_{-j} e^{-\underline{k}l} + \underline{v}_{+j} e^{\underline{k}l}\right] = 0,\\
\underline{F}(l) &\equiv \frac{B\underline{k}^3}{j\omega}\left[j\underline{v}_+ e^{-j\underline{k}l} - j\underline{v}_- e^{j\underline{k}l} - \underline{v}_{-j} e^{-\underline{k}l} + \underline{v}_{+j} e^{\underline{k}l}\right] = 0,\\
\underline{M}(0) &\equiv -\frac{B\underline{k}^2}{j\omega}\left[-\underline{v}_+ - \underline{v}_- + \underline{v}_{-j} + \underline{v}_{+j}\right] = 0,\\
\underline{F}(0) &\equiv \frac{B\underline{k}^3}{j\omega}\left[j\underline{v}_+ - j\underline{v}_- - \underline{v}_{-j} + \underline{v}_{+j}\right] = \underline{F}_0.
\end{aligned} \tag{4.43}$$

By solving Eq. (4.43) for the four unknowns, one finds after some lengthy manipulation that bending vibrations of free-free beams obey

$$\underline{v} = \frac{j\omega \underline{F}_0}{\underline{B}\underline{k}^3} \frac{\begin{array}{c}\sinh \underline{k}l \cos \underline{k}(l-x) - \sin \underline{k}x - \cosh \underline{k}l \sin \underline{k}(l-x) \\ -\sin \underline{k}l \cosh \underline{k}(l-x) + \sinh \underline{k}x + \cos \underline{k}l \sinh \underline{k}(l-x)\end{array}}{2(1-\cos \underline{k}l \cosh \underline{k}l)}. \tag{4.44}$$

For the location $x = l$, this result reduces to

$$\underline{v}(l) = \frac{j\omega \underline{F}_0}{\underline{B}\underline{k}^3} \frac{\sinh \underline{k}l - \sin \underline{k}l}{1 - \cos \underline{k}l \cosh \underline{k}l}. \tag{4.45}$$

When $kl \to 0$ i.e., for very short beams, one may show by using a series expansion including terms up to the fourth power of $(kl)$ that

$$\underline{v}(l) \approx \frac{2\underline{F}_0}{j\omega m'l}. \tag{4.45a}$$

This result corresponds to rigid-body motion including rotation and translation of a rigid beam excited laterally at one end.

Figure 4.8a shows how the velocity at the end $x = l$ varies with frequency, as calculated from Eq. (4.45). Figure 4.8b shows how the velocity varies along the beam at a constant frequency corresponding to $k'l = 9\pi/2$, as calculated from Eq. (4.44). In these figures the ordinate again is the logarithm of the absolute value of the velocity, and the abscissa are $k'l$ and $k'x$, respectively. Because $k' = \sqrt{\omega}\ \sqrt[4]{m'/B}$, the abscissa of Fig. 4.8a is proportional to the square-root of the frequency.

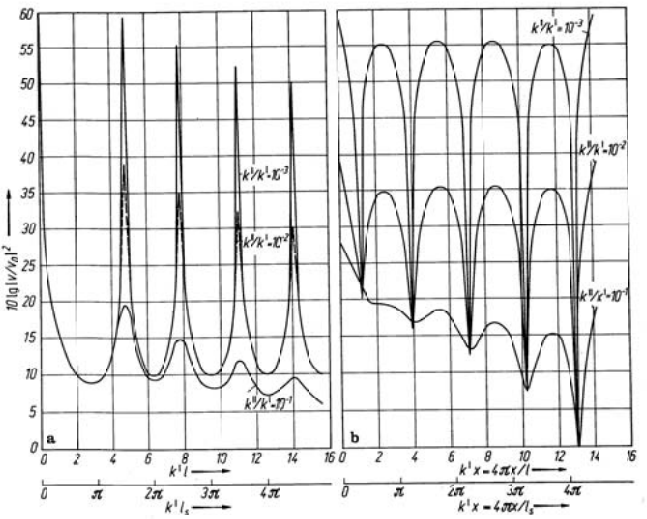


**Fig. 4.8.** Flexural vibrations of a free-free beam. a) Variation with frequency at $x = l$, as calculated from Eq. (4.45); b) Variation with position, for $k'l = 9\pi/2$, as calculated from Eq. (4.44)

One may derive Eq. (4.45) – but not Eq. (4.44) – considerably more rapidly with the aid of the so-called eight-pole equations [4.8]. In order to develop these equations conveniently, one may rewrite Eq. (4.42a) in terms of the following functions:

$$\frac{1}{2}\left(\cosh kx+\cos kx\right)=C\left(kx\right),\quad \frac{1}{2}\left(\cosh kx-\cos kx\right)=c\left(kx\right),$$
$$\frac{1}{2}\left(\sinh kx+\sin kx\right)=S\left(kx\right),\quad \frac{1}{2}\left(\sinh kx-\sin kx\right)=s\left(kx\right).$$

These functions have the property that differentiation of any of them gives another function of the set, in the sequence $C\,(kx)$, $s\,(kx)$, $c\,(kx)$, $S\,(kx)$, $C\,(kx)$. In addition $C\,(0) = 1$, $S\,(0) = s\,(0) = c\,(0) = 0$. If the transverse velocity and the angular velocity are written as

$$\underline{v}_x=\alpha C\left(kx\right)+\beta S\left(kx\right)+\gamma\, c\left(kx\right)+\delta\, s\left(kx\right)$$
$$\underline{w}_x=k\left[\alpha s\left(kx\right)+\beta C\left(kx\right)+\gamma\, S\left(kx\right)+\delta\, c\left(kx\right)\right],$$

one may observe that the velocity $v_0$ at the beginning of the beam is equal to $\alpha$, whereas the angular velocity at the beginning of the beam is $w_0 = k\beta$. The moment and the shear force similarly may be found to be simply related to the coefficients in the foregoing expressions. After some mathematical manipulation, one may determine that

$$\begin{aligned}
\underline{v}_x &= \underline{v}_0 C\left(kx\right)+\underline{w}_0\frac{1}{k}S\left(kx\right)-\underline{M}_0\frac{1}{jW'}c\left(kx\right)+\underline{F}_0\frac{1}{jW'k}s\left(kx\right)\\
\underline{w}_x &= \underline{v}_0 ks\left(kx\right)+\underline{w}_0 C\left(kx\right)-\underline{M}_0\frac{k}{jW'}S\left(kx\right)+\underline{F}_0\frac{1}{jW'}c\left(kx\right)\\
\underline{M}_x &= -\underline{v}_0 jW'c\left(kx\right)-\underline{w}_0\frac{jW'}{k}s\left(kx\right)+\underline{M}_0 C\left(kx\right)-\underline{F}_0\frac{1}{k}S\left(kx\right)\\
\underline{F}_x &= \underline{v}_0 jW'kS\left(kx\right)+\underline{w}_0 jW'c\left(kx\right)-\underline{M}_0 ks\left(kx\right)+\underline{F}_0 C\left(kx\right),
\end{aligned}\tag{4.46}$$

where $W' = Bk^2/\omega = \sqrt{Bm'}$.

Inversion i.e., expressing the parameters at the beginning of the beam in terms of those at the end may easily be accomplished here (as for the four-pole equations), because the determinant of the coefficients is equal to unity, in view of reciprocity. Here, the inversion merely leads to a change in the algebraic sign of the $S\,(kx)$ and $s\,(kx)$ terms.

Several approximations are of interest in relation to experimental measurements. For $k'l > \pi$, the variation with frequency of the velocity at the $x = l$ end of the beam may be written as

$$\left|\underline{v}(l)\right|^2 \approx \left|\frac{\omega \underline{F}_0}{B\underline{k}^3}\right|^2 \frac{2}{\cosh 2k''l + \cos 2k'l}, \tag{4.47}$$

and the spatial variation in the region $\pi < k'x < k'l - \pi$ may be approximated by

$$\left|\underline{v}(x)\right|^2 \approx \left|\frac{\omega \underline{F}_0}{B\underline{k}^3}\right|^2 \frac{\cosh 2k''(l-x) - \sin 2k'(l-x)}{\cosh 2k''l + \cos 2k'l}. \tag{4.48}$$

It is easily verified that these equations are also obtained by setting $\underline{r}_0 = \underline{r}_l = -j$ in Eq. (4.27). As has already been mentioned, one may apply the simpler relations of Sect. 4.3.1 to bending vibrations of long beams, if one introduces the appropriate reflection coefficients. The differences between the different wave types only become evident if one determines the frequencies and the loss factor from the wavenumbers $k'$ and $k''$. For bending waves one find $k''/k' = \eta/4$ (see Eq. (4.12b)), unlike for longitudinal and torsional waves.

The damping of bending waves can be determined from half-value bandwidth measurements, exactly as for longitudinal and torsional waves, provided the beam is not too highly damped. The same analysis as was carried out in Sect. 4.3.1 in this case leads to

$$\frac{\underline{v}_B}{\underline{v}_{\max}} \approx \frac{1}{1 + j\dfrac{\Delta k'l}{k''l}}. \tag{4.49}$$

Because $k = \sqrt{\omega}\sqrt[4]{m'/B}$, one finds that here $\Delta k = \dfrac{1}{2}\dfrac{k\Delta f}{f_n}$. Thus,

$$\left|\frac{\underline{v}_B}{\underline{v}_{\max}}\right|^2 \approx \frac{1}{1 + \left(\dfrac{2\Delta f}{\eta f_n}\right)^2}. \tag{4.49a}$$

One may observe that the relation between bandwidth and loss factor for bending waves is the same as that for longitudinal and torsional waves, namely,

$$b = \eta f_n. \tag{4.50}$$

The vibrations in the vicinity of a vibration node obey the same relations as derived in Sect. 4.3.1. Therefore Eqs. (4.37) to (4.39) apply directly to bending waves, for locations outside of the nearfield regions.

The behaviour of beam vibrations in the vicinity of the various resonances is of interest not only in relation to experiments and for determination of the loss factor, but also because any vibration of a beam can be rep-

resented by a sum of its resonant or natural vibrations. This problem is treated in detail in Sect. 5.7, where it is shown that the velocity of a beam may be expressed as

$$\underline{v}(x) = \sum_{n=0}^{\infty} \frac{\underline{v}_n \varphi_n(x)}{\omega_n^2 (1 - j\eta) - \omega^2}. \tag{4.51}$$

Herein, $\omega_n$ represent the radian natural frequencies of the beam, the $\underline{v}_n$ are coefficients which are relatively independent of the frequency, and $\varphi_n(x)$ represent the so-called eigenfunctions or mode shapes. Equation (4.51) applies for longitudinal and torsional waves, as well as for bending waves; one only needs to use the appropriate values for $\omega_n$, $\underline{v}_n$ and $\varphi_n(x)$.

It may seem somewhat surprising at first glance that the velocities given by Eqs. (4.44) or (4.27) can be represented by an expression like that in (4.51), because these equations have entirely different forms. However, one may change one of these equations to the other by use of the Mittag-Leffler theorem of function theory, which states that every meromorphic function and thus also the functions $1/\sin x$ and $1/\cos x$ may be represented by an infinite sum. The actual transformation of one equation into the other involves no difficulty in principle, but is too tedious to be carried out explicitly here.

Equation (4.49a), which is most important in relation to loss factor measurement, can be obtained directly from Eq. (4.51) by neglecting all but the largest term and considering only a single point $x = x_0$. In this manner one finds

$$\underline{v}(x_0) \approx \frac{\underline{v}_n \varphi_n(x_0)}{\omega_n^2 - \omega^2 - j\omega_n^2 \eta} = \frac{\underline{v}_n \varphi_n(x_0)}{(\omega_n - \omega)(\omega_n + \omega) - j\omega_n^2 \eta}. \tag{4.52}$$

In the vicinity of a resonance, $\omega = \omega_n$, $\omega_n + \omega \approx 2\,\omega_n$ and with $\omega_n - \omega = \Delta\omega$, it is found that

$$\underline{v}(x_0) \approx \frac{\underline{v}_n \varphi_n(x_0)}{-j\omega_n^2 \eta} \frac{1}{1 + j\dfrac{2\Delta\omega}{\eta\omega_n}},$$

which corresponds directly to Eq. (4.49a).

## 4.4. Measurement of Complex Moduli

Because the complex modulus of elasticity of a material is a very important mechanical property, many techniques are available for its measure-

ment. Only the most important ones will be described here. In essence, there exist three basically different types of measurement methods. For low-frequency measurements on a sample of small dimensions, one may consider the test sample as a spring; one then needs only to determine the sample's spring constant. At intermediate and high frequencies, this approach ceases to work, because the sample then acts more like a wave-carrying distributed system than an ideal (mass-less) spring. In this upper frequency region, one therefore uses rod-shaped test samples and deduces the mechanical properties of the sample from the behaviour of longitudinal, torsional and bending waves. At very high frequencies, particularly in the ultrasonic region, where the wavelengths usually are considerably smaller than all sample dimensions, one generally determines material data by considering the test samples to be semi-infinite continua.

Only the first two types of measurements will be discussed here; for information on pure ultrasonic measurements the reader is referred to the specialized literature on the subject [4.9]. Also, no attempt will be made here to discuss the relation between mechanical properties and the structure of matter, although such topics have been the subject of great activity in the past few years and include many interesting effects e.g., coupling between sound and electron motions. Such topics belong the to field of pure physics and appear to have little application to noise control practice. On the other hand, investigations of the structure of high-polymer materials by means of structure-borne sounds measurements have led to the development of materials, which are of direct interest for structure-borne sound attenuation purposes, and such materials will be discussed in some detail.

## 4.4.1 Measurements on Small Samples

### *4.4.1.1 Stress-Strain Curve*

A direct method for determination of the complex modulus of elasticity is shown schematically in Fig. 4.9. The test sample is rigidly fixed at one end, and excited by a periodic force $F$ at the other. From the absolute values of the force and of the resulting displacement $\Delta\xi$ one may determine the absolute value of the modulus of elasticity from

$$\frac{|F|}{|\Delta\xi|} = |\underline{E}|\frac{S}{l} = \frac{S}{l}E'\sqrt{1+\eta^2}. \tag{4.53}$$

*S* represents the cross-sectional area and *l* the length of the test sample and from the phase angle φ between the force and the displacement one may find the loss factor as

$$\eta = \tan \varphi. \tag{4.54}$$

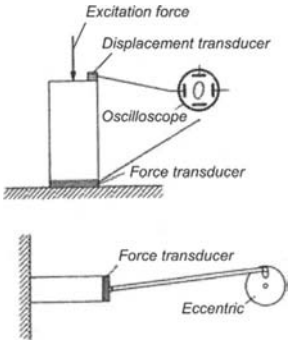


**Fig. 4.9.** Measurement of complex modulus via the stress-strain curve

Usually, electrodynamic shakers are most convenient for providing the required oscillatory force, and electromechanical transducers are used for sensing force and displacement. It thus is relatively easy to convert all mechanical quantities into electrical ones, to amplify without introducing significant phase shifts, and to measure them. For the signal processing, real-time FFT-analyser are suitable and furnishes readily the frequency response function sought, cf. Sects. 2.1 and 5.2. A frequency response function defined as the complex ratio of force to displacement represents directly the complex dynamic stiffness sought. Somewhat more physically direct perhaps but significantly more time consuming is the employment of an oscilloscope where the excitation and response signals are fed to the horizontal and vertical plates of the cathode ray tube. The oscilloscope output is an ellipse from which the real and imaginary parts of the complex modulus can be determined as given by Eq. (4.20) and illustrated in Fig. 4.4. In addition, one may easily recognize irregularities such as nonlinearities due to buckling of the test sample, higher order vibrations, resonances in the support system from distortions of the ellipse.

One may also excite the test sample in bending or torsion and deduce the complex bending stiffness and the complex shear modulus from the measured forces, moments, and translational or rotational displacements. Instead of applying a periodic force, one may also apply a periodic dis-

placement, for example, by means of an eccenter, see the lower part of Fig. 4.9. This arrangement also permits the application of a static preload without great difficulty.

The most significant problems with this type of measurement are associated with the accuracy to which the phase angle must be measured and with supporting the sample "rigidly". A "rigid support" is just as impossible to realize as, e.g., an absolute vacuum. In order to measure loss factors of the order $\eta \approx 10^{-2}$ with a 10 % accuracy, a value typical for example, for wood, the accuracy with which the phase angle between the force and displacement must be determined should be better than 0.6 degrees. Although, high-performance electronic equipment can achieve such an accuracy, losses in the sample support commonly contribute with larger phase shifts. Therefore, the applicability of the method is limited to relatively soft material with not too small loss factors such as rubber [4.10]. The lowest resonance frequency of the measurement set-up, moreover, must of course be considerably above the highest frequency of interest. Attention must also be paid the fixturing of the sample end. Upon applying a clamping support, the length of the test sample is no longer precisely defined since also the clamped part of the sample will participate in the deformation. It is thus advisable to use slender samples where such end effects are comparatively small. Unfortunately, slender samples are prone to buckling. If, on the other hand, use is made of short pad-shaped test samples other problems are introduced. For instance, the cross-sectional contraction of the sample is impeded at the contact area with the support yielding a locally enlarged modulus of elasticity. In particular, this effect must be considered for rubber samples where the Poisson's ratio is close to 0.5.

The length of the sample imposes a limit on the applicability of this measurement technique. As shown by Eq. (4.29), the stiffness of a sample that is clamped at one end is given by $\omega Z \cot kl$. Because $kl = 2\pi l/\lambda$, Eq. (4.53) ceases to apply if the length of the test sample approaches the longitudinal wavelength or the bending or torsional wavelength, in bending or torsional tests. From a series expansion of cot $kl$ one may find that the fractional error due to the finite length of the sample is of the order of $k^2l^2/3$. For a sample whose length is $1/50^{\text{th}}$ of the wavelength, this error is about 0.5 percent whereas for a sample length $1/10^{\text{th}}$ of the wavelength, the error amounts to 13 percent.

The method described above has one great advantage; namely, it permits one to change the measurement frequency continuously without changing the sample. One may thus determine the frequency dependence of the modulus and of the loss factor without difficulty over the entire measurement range of the apparatus. This is not the case for all the resonance methods.

### 4.4.1.2 Frequency Response Measurements in a Mass-Spring-Mass Rig

Due to the large difficulties in realizing a rigid support as employed in Fig. 4.9, is commonly used a measurement rig with dynamically free terminals. The simplest form of such a rig is the mass-spring-mass system. Two examples of such a rig type are shown in Fig. 4.10. When the masses can be considered rigid, the spring element comparatively "mass-less" and the suspension of the rig itself as well as that of any static preload dynamically free, the equations of motion read

$$\begin{aligned} j\omega m_1 \underline{v}_1 + \frac{\underline{s}}{j\omega}\left(\underline{v}_1 - \underline{v}_2\right) &= \underline{F}_0, \\ j\omega m_2 v_2 + \frac{\underline{s}}{j\omega}\left(\underline{v}_2 - \underline{v}_1\right) &= 0. \end{aligned} \tag{4.55}$$

This means that all the suspensions are made extremely soft such that there is no dynamic interference in the measurement range from the support or preload body.

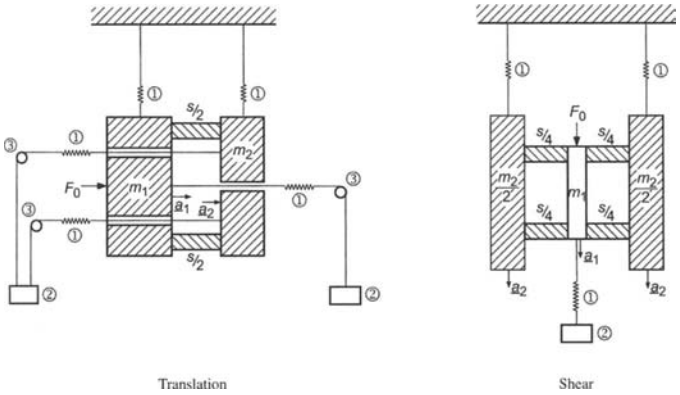


**Fig. 4.10.** Measurement of frequency response functions $a_1/F_0$, $a_2/F_0$ or transfer function $a_1/a_2$, in a mass-spring-mass system. ① suspension, ②preload and ③ pulleys

From Eq. (4.55) is obtained

$$\begin{aligned} \underline{v}_1 &= \underline{F}_0 \frac{j\omega m_2 + \underline{s}/\, j\omega}{\underline{s}\left(m_1 + m_2\right) - \omega^2 m_1 m_2}, \\ v_2 &= \underline{F}_0 \frac{\underline{s}/\, j\omega}{\underline{s}\left(m_1 + m_2\right) - \omega^2 m_1 m_2}. \end{aligned} \tag{4.56}$$

As can be seen, there is an antiresonance at $\omega_A^2 = s/m_2$ which means that the velocity $v_1$ vanishes. Also, a resonance occurs at $\omega_R^2 = \underline{s}(m_1 + m_2)/m_1 + m_2$. At those two frequencies, the dynamic stiffness can be determined from Eq. (4.56). A more direct way to determined the dynamic stiffness, however, is obtained via the frequency response functions $\underline{a}_1/\underline{F}_0$ and $\underline{a}_2/\underline{F}_0$ or via the transfer functions $\underline{a}_1/\underline{a}_2$. Introducing $\underline{a} = j\omega\underline{v}$ instead of the velocities in Eq. (4.56) yields

$$\begin{aligned}
\underline{s} &= \omega^2 m_2 \frac{1 - m_1 \underline{a}_1 / \underline{F}_0}{1 - (m_1 + m_2)\underline{a}_1 / \underline{F}_0}, \\
\underline{s} &= -\omega^2 m_2 \frac{m_1 \underline{a}_2 / \underline{F}_0}{1 - (m_1 + m_2)\underline{a}_2 / \underline{F}_0}, \\
\underline{s} &= \omega^2 m_2 \frac{1}{1 - \underline{a}_1 / \underline{a}_2}.
\end{aligned} \tag{4.57}$$

Of the above forms, the last is the most convenient since it only involves the acceleration ratio and only requires a simple calibration.

The lower limiting frequency is set by the stiffness of the elastic suspension and 1 Hz is possible without greater difficulty. It should be observed the losses in the suspension elements should small in order not to influence the measurements. Such a suspension, for example, can be realized by means of air springs (balloon). The upper frequency limit is given by the eigen-frequencies of the masses. which most often corresponds to bending resonances. It is preferable to try to achieve as symmetric a rig as possible to avoid rotational oscillations. Advisable is to ascertain the amount of contamination due to such rotations prior to the actual test or to perform a modal analysis.

The influence of sample size in comparison with the wavelength, as mentioned in Sect. 4.4.1.1, is also important for measurements in a mass-spring-mass rig. It can be reduced by adding the mass of the test sample proportionally to the two masses.

Which of the three forms in (4.57) is the more suitable depends on the specific case. In any case is a situation with $\underline{a}_1 \approx \underline{a}_2$ always problematic with respect to the last form since the difference in the denominator becomes small.

The measurement of moduli via transfer functions is due to Fitzgerald [4.11] who used a specific rig. Hereby, the mechanical quantities are proportional to electrical resistances, accurately determined from a bridge-circuit.

### 4.4.1.3 Vibration Decay

Whereas the previously discussed methods involve measurements of both stresses and strains, only one variable (usually the strain, velocity, or acceleration) needs to be measured in all techniques based on resonances of a system. However, these techniques have the disadvantage that one can obtain data at only one frequency, namely the resonance frequency.

A well-known technique of this type makes use of a torsion pendulum (Fig. 4.11). This technique is often used for measurements on high-polymer materials at low frequencies, but is not limited to such materials. To avoid tension of the test sample due to the disc mass, the latter is placed on top and suspended by a string.

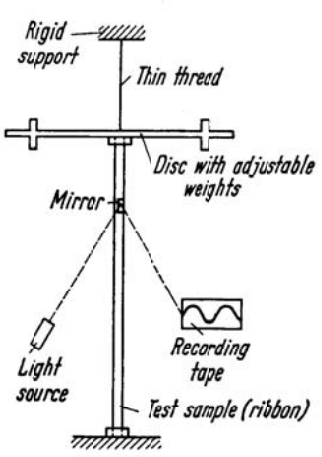


**Fig. 4.11.** Schematic arrangement of torsional pendulum

In tests of this type use was earlier made of an optical arrangement consisting of a light source, a small mirror, and recording paper which moves past a window at a constant velocity. The vibrations are recorded directly on this paper, and one may, for example, determine the natural frequency $f_0$ directly from the distance between the peaks and the known paper speed. For higher frequencies, however, electrical measurements are usually employed. The damping is usually determined in terms of the so-called logarithmic decrement. $\Lambda$, which is defined as the logarithm of the ratio of successive maxima. If $A_n$ represents the maximum excursion measured at a certain time, and if $A_{n+1}$ represents the maximum excursion at one period later, then $\Lambda$ is defined as

$$\Lambda = \ln\left(A_n / A_{n+1}\right). \tag{4.57a}$$

For small damping, one finds from Eq. (4.24) that

$$\eta = \Lambda / \pi \ . \tag{4.58}$$

For large damping, inclusion of a correction leads to

$$\eta = \frac{\Lambda / \pi}{\sqrt{1 + \left(\Lambda / 2\pi\right)^2}}. \tag{4.59}$$

Because $\Lambda$ can be determined rather accurately from measurement over several periods, the vibration decay technique is a simple and reasonably exact method for the loss factor $\eta$.
The second quantity of interest, the torsional stiffness $T$ of the sample, is given by

$$|T| = \left(2\pi f_n\right)^2 \Theta \left(1 + \frac{\Lambda^2}{4\pi^2}\right), \tag{4.60}$$

where $\Theta$ represents the mass moment of inertia of the disc. The absolute value of the shear modulus is determined from the torsional stiffness and the dimensions of the sample. For ribbon-shaped test samples, as are often used,

$$|\underline{G}| = G' \sqrt{1+\eta^2} = |T| \frac{3l}{b^3 h\left(1 - 0.63 b/h\right)}, \tag{4.61}$$

where $l$ represents the length, $h$ the width, and $b$ the thickness of the test sample with $h > b$. (For high-polymers, the German standard DIN 53445 recommends ribbon dimensions $l \approx 60$mm, $h \approx 10$mm, $b \approx 2$mm.) For the relation between torsional stiffness and shear modulus, see also Table 3.1 and Eq. (3.64).

The primary advantage of the torsional pendulum is its great simplicity. It allows tests at many temperatures in a relatively short time, but suffers from the disadvantage that with a given sample and disc moment of inertia $\Theta$ one can obtain data at only one frequency. One can determine the frequency dependence of the modulus only rather inconveniently, by changing $\Theta$, $l$, $b$, and $h$. There is virtually no lower limit for the frequency at which a torsion pendulum can be used, provided that the large discs that are needed to produce low frequencies can be made not to load the test sample excessively. Frequencies of 0.1 Hz are attainable without great difficulty.

The highest frequency at which a torsion pendulum is useful depends on the length of the test sample; for a measurement accuracy of 1 %, this length must not exceed 1/50 th of the torsional wavelength. Useful data above 500 Hz are rarely achieved with a torsion pendulum.

#### 4.4.1.4 Resonance Frequency and Half-Value Bandwidth

The various test arrangements, in which the test sample acts as the spring in a resonant mechanical system, are closely related to the torsion pendulum in principle but differ considerably in configuration. In such set-ups, which are widely used for testing of fiber mats, foam materials, cork, etc., typically one end of the sample is fastened to a rigid support or to a large, very softly supported mass. To the other end of the sample is attached a known mass; the mass is excited by an oscillating force, and the velocity of the mass is sensed by means of a suitable transducer, see Fig. 4.12. By varying the frequency of the exciting force while holding the amplitude of the force approx. constant, a resonance frequency $f_R$ is observed, and usually the corresponding half-value bandwidth $b$ can be measured without great difficulty.

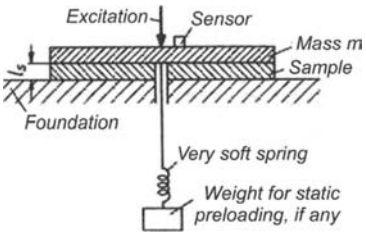


**Fig. 4.12.** Measurement of dynamic stiffness and loss factor via resonance frequency and bandwidth

The real part of the modulus of elasticity may be calculated from

$$E' = 4\pi^2 f_R^2 m \frac{l}{S}, \tag{4.62}$$

where $l$ represents the thickness of the sample and $S$ its surface area. For a sample resting on a rigid support, $m$ represents the mass atop the sample. For a test sample resting on a softly supported mass $m_u$ and carrying a mass $m_0$, $m$ is given by $m = m_0 m_u/(m_0 + m_u)$ cf. Fig. 4.10. When the mass

of the test sample $m_s$ cannot be neglected, a first correction can be made by adding $m_s/3$ to the mass $m$ for a set-up as in Fig. 4.12 whereas the sample mass is proportionally added to the two masses of the mass-spring-mass set-up. The loss factor is given by

$$\eta = \frac{b}{f_R} \,. \tag{4.63}$$

To achieve a higher accuracy in the measured loss factor, it is appropriate to plot the velocity ratio $|v_m/v_{m,\,max}|^2$ versus the square of the frequency shift $(\Delta\omega)^2$, cf. Eq. (8.22). In this way a straight line results which slope is proportional to the decay constant $\delta$, from which the loss factor is obtained as $\eta = \delta/\pi f_r$.

In order to investigate the properties of the sample at various frequencies, one must change the mass supported by the sample. Quite often it does not suffice simply to lay additional weights atop the initial one; the weights must usually be bolted together or rigidly interconnected some other way, so that the total mass $m$ acts as a single rigid body without resonances of its own. (One may also preload the sample statically – for example, in order to investigate the load-dependence of the behaviour of a foam mat – by connecting additional weights to the weight supported by the sample via a very soft spring, as indicated in Fig. 4.12.)

Like all measurement methods in which the loss factor is determined from the half-value bandwidth, the present method is useful only for small loss factors. If the loss factor is too large, the resonance curve becomes so flat that the bandwidth no longer can be discerned. In the best case, the relative error is of the order $\eta^2/2$.

Again, the range of applicability of the arrangements discussed here is limited by the sample thickness, which must be much smaller than the corresponding wavelength.

Practical difficulties in the use of such test arrangements also arise because of resonances of the supports and rocking motions of the sample, caused by unsymmetrical excitation. Both of these effects make it difficult to measure a single, clearly defined resonance, and thus to determine an unambiguous stiffness. In addition, care must be taken to ensure that the excitation system does not introduce extraneous damping. The damping of samples of materials that contain air (fibre mats or foams) sometimes depends markedly on sample size and geometry. For samples that have only open pores, one measures the stiffness of only the matrix material if one uses small samples and low frequencies; the air then is merely “pumped” in and out. At high frequencies, the air can no longer be moved back and forth rapidly enough; it then suffers some compression and may make a

considerable contribution to the total stiffness. For samples with closed cells, one cannot distinguish between the stiffness of the material itself and that of the enclosed air; one can only measure the total stiffness, which – like that of rubber – depends very strongly on the geometry of the sample. Such samples may behave much like liquids, i.e., they may exhibit a Poisson's ratio near 0.5.

### 4.4.2 Measurements on Beams

As was discussed in detail in Chapter 3, on beams are encountered primarily quasi-longitudinal waves, torsional waves, and bending waves. Surface waves occur only at relatively high frequencies. Thus, one may use the three aforementioned types of waves for measurements on beams. In practice, one usually concerns oneself only with bending waves, not only because these are most important with respect to sound radiation, but also because they can be excited most easily and most "cleanly" since their impedance is the smallest of those of the three wave types. The available bending-wave measurement techniques have been develop primarily for studying damping layers and similar noise control treatments [4.12, 4.13]. These techniques will be discussed in some detail in the following paragraphs. Techniques pertaining to torsional and quasi-longitudinal waves will be treated only cursorily.

#### *4.4.2.1 Half-Value Bandwidth*

Bending-wave resonances can be measured best on freely suspended beams, with excitation applied to one end and the resulting vibrations observed at the other, as shown schematically in Fig. 4.13.

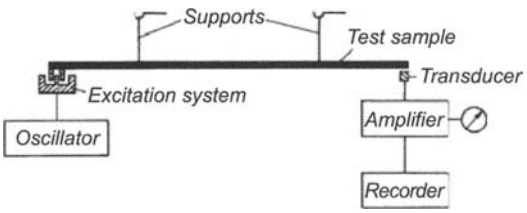


**Fig. 4.13.** Measurement of flexural resonance frequency and bandwidth

In this arrangement, the exciter and the sensor are at an anti-node at all frequencies; one thus avoids the difficulties associated with (frequency dependent) standing waves. Almost any electromechanical system that can be loosely coupled to the test specimen may be used as an exciter; even the electro-magnet from an earphone and a razorblade glued to the test beam will do. The loose coupling is important, because the test sample must not be damped or loaded by the excitation system. The same also holds for the sensor system. For very light samples, a capacitative sensor is usually best (a microphone mounted within 1/2 to 1 mm from the surface of the beam, in order to sense the airborne sound associated with the vibrations, constitutes an acceptable makeshift device). For large samples, other sensors may also be used. If the sensor is not to distort the measurements, its mass must be less than $M/30\ n$, where $M$ represents the total mass of the sample beam and $n$ is the number of vibration nodes on the beam at the highest frequency of interest. Thereby, it is presumed that the mass impedance of the transducer is smaller than a tenth of the point impedance of the beam, cf. Sect. 5.3.2. One may use a somewhat heavier sensor, if one is not interested in the exact values of the higher resonance frequencies.

The suspension of the sample must be arranged so that it introduces no extraneous damping. If the loss factors to be measured are greater than $10^{-3}$, then one usually may obtain acceptably low support damping simply by suspending the beam from threads in any convenient manner. For smaller loss factors and light samples, however, one must support the beam at nodal points, in order to minimize the vibratory energy extracted from the beam by the suspension system; the supports then must be moved for different resonances, see Fig. 4.13. Radiation of acoustic energy to the surrounding air may also contribute extraneous damping which is significant if one desires to measure small loss factors ($\eta < 10^{-4}$). One may reduce this radiation damping by choosing the test sample shape appropriately – or, of course, by carrying out the measurements in a vacuum. A practically simple arrangement is to insert the test sample in an upside-down-held plastic bag filled with helium, cf. [4.14].

One may determine the complex modulus simply by measuring the resonance frequencies $f_n$ and the corresponding half-value bandwidths $b$. A typical amplitude-frequency curve is shown in Fig. 4.14.

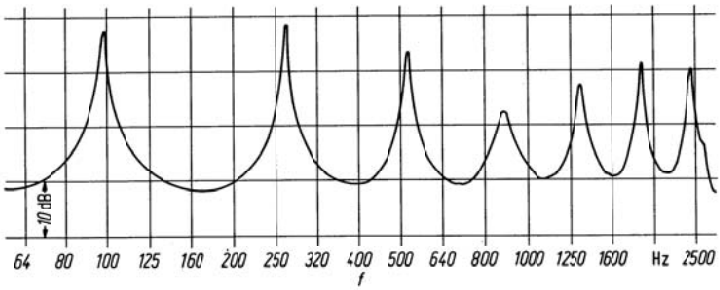


**Fig. 4.14.** Experimentally determined vibration response of a free-free beam (with a thin damping layer; $\eta \approx 2 \times 10^{-2}$, frequency dependent)

In view of Eq. (3.111e), the real part of the bending stiffness is found from

$$B' = m'l^4 f_n^2 \frac{64}{\pi^2 (2n-1)^4}. \tag{4.64}$$

and the loss factor from

$$\eta = \frac{b}{f_n}, \tag{4.65}$$

where $m'$ represents the mass per unit length of the test beam, $l$ represents its length such that $m'l$ is the total mass, $n$ is the number of nodes, which can be determined by scanning the distribution of vibrations along the beam.

Equation (4.64) is not exact, because it neglects the slight reduction in the resonance frequency that is caused by the damping. The fractional error in the frequency associated with this approximation amounts at most to $\eta/4$ (see remarks in relation to Eq. (4.32)), but is never of great importance, because the resonance method allows measurements of loss factors only up to about 0.1. This limit stems from the fact that for large losses the vibration field is no longer resonant. Fig. 4.8a shows that for $k''/k' = 0.1$ i.e., $\eta \approx 0.4$, the rise in level hardly becomes more than 3 dB already at the third resonance. A consideration of high order terms shows that the representation of beam vibrations through a resonance curve i.e., the use of Eq. (4.49) instead of (4.47), is fully inappropriate for $k''l > 1$. The fractional error in $\eta$ is approximately $n^2\eta^2/5$ in other words, if the frequency interval between resonances is of the same order as the half-value bandwidth, then one can no longer use this method.

#### 4.4.2.2 Decay Time

For very small damping, one generally obtains more accurate results by measuring decay or reverberation times than by measuring half-value bandwidths. For $f$ = 100 Hz and $\eta = 10^{-3}$, for example, the half-value bandwidth is only 0.1 Hz and thus cannot readily be measured by means of some simple apparatus. The same arrangement as described in the previous section may be used for decay measurements. Instead of determining how the amplitude varies with frequency in the vicinity of resonances, however, the decay of the vibrations is observed after the excitation is suddenly turned of. As is evident from Eq. (4.24), energy decay may be described by the function $e^{-\eta\omega t}$. Thus, the reverberation time $T$ (within which the energy of the vibration is reduced to one millionth of its initial value) is measured as in room acoustics, and the loss factor is determined from the relation

$$\eta = \frac{\ln 10^6}{\omega T} \approx \frac{2.2}{f T}, \tag{4.66}$$

which follows from Eq. (4.24). One may, of course, also measure any other parameter that characterizes the decay process, instead of the reverberation time $T$, and compute $\eta$ from it.

If only the loss factor is of interest and not also the bending stiffness, then only the reverberation time need be measured, for example, resulting from exciting the test sample by hammer impacts. In order to determine the frequency dependent of the loss factor, one must then filter the electrical signal picked up by the sensor. This measurement process does not yield particularly accurate results, because two or more natural vibrations with different decay times may lie within a filter bandwidth, leading to broken reverberation curves, from which the loss factor cannot be determined uniquely.

Irregularities in decay processes may also occur with periodic excitation namely, if the excitation frequency does not quite coincide with the natural frequency, see Fig. 4.15. Equation (4.24) was derived under the assumption that only one energy reservoir is present. If this is not the case, e.g., if two types of waves or several natural vibration modes are excited simultaneously as occurs with off-resonance excitation, then it may happen that mechanical energy is not only changed to heat, but also exchanged back and forth between two or more energy reservoirs, leading to rather remarkable decay curves.

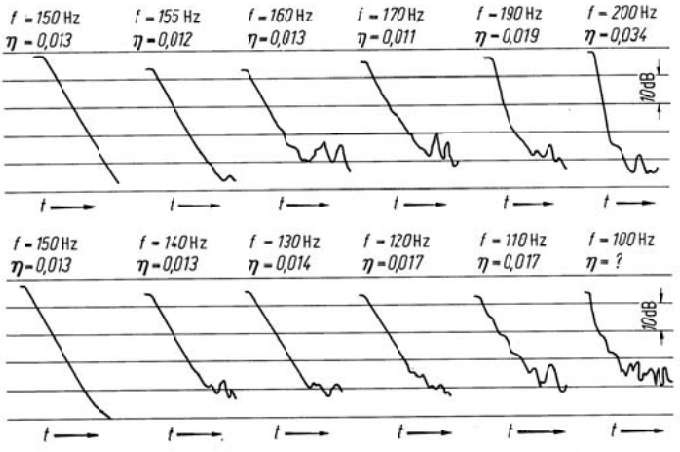


**Fig. 4.15.** Experimentally observed decay process near a resonance frequency of 150 Hz

In principle, reverberation time measurements are applicable up to relatively high values of the loss factor η. However, because of the inertia of the usual instrumentation, this technique generally is useful only for small damping.

### *4.4.2.3 Attenuation of Vibrations with Distance*

In the limiting case of very long, highly damped beams, wave propagation occurs as on infinitely long beams. The velocities (or acceleration) at the two points $x_0$ and $x_1$ are related by

$$\underline{v}_1 = \underline{v}_0 e^{-j\underline{k}(x_0 - x_1)} = \underline{v}_0 e^{-k''(x_0 - x_1)} e^{-jk'(x_0 - x_1)}. \tag{4.67}$$

Thus, the phase difference between these two points is given by

$$\varphi_{01} = k'(x_1 - x_0) = \frac{2\pi}{\lambda}(x_1 - x_0), \tag{4.68}$$

where λ represents the wavelength, and the reduction in amplitude obeys

$$\ln \frac{v_0}{v_1}\,\mathrm{Np} = 10 \log \frac{|v_0^2|}{|v_1^2|}\,\mathrm{dB} = 8.7 k''(x_1 - x_0)\,\mathrm{dB}. \tag{4.69}$$

By measuring the phase and the amplitude reduction one may therefore determine the real and imaginary parts of the wave number.

For damping that is not extremely high, one may obtain the real part of the bending stiffness from

$$B' = \omega^2 m' \frac{1}{k'^4} = \omega^2 m' \left( \frac{x_1 - x_0}{\varphi_{01}} \right)^4 \tag{4.70}$$

and the loss factor from

$$\eta = 4 \frac{k''}{k'} = \frac{D'_B \lambda}{13.6}, \tag{4.71}$$

where $D'_B$ represents the reduction in vibration level in decibels per unit length, that is, $(x_1 - x_0) D'_B = 10 \log \left[ |v_0|^2 / |v_1|^2 \right] \text{dB}$.

In order to carry out this measurement, one typically excites the test beam at one end and scans the vibrations along the rod with a movable sensor as depicted in Fig. 4.16.

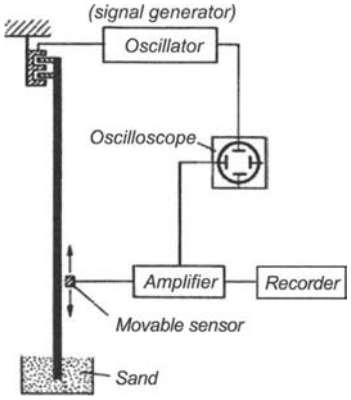


**Fig. 4.16.** Scanning of propagating flexural waves for measurement of wavelength and damping

If one moves the scanning sensor along the beam at a constant velocity, then one may determine $D'_B$, and thus $k''$, directly from the slope of the recorded vibration level. Measurement of the phase difference may be accomplished simply by feeding the exciting voltage and the signal from the sensor to the two perpendicular pairs of plates of an oscilloscope and by marking on the test beam the points at which the phase difference with respect to the excitation amounts to 180° or 360°. Naturally, the phase can be registered directly also by means of a two-channel signal analyser.

Suspension of the test sample and attachment of the exciter is relatively uncritical for this type of measurement, but the scanning sensor must be relatively light. It is usually useful to embed one end of the beam in sand or some similar material, in order to reduce the reflection of waves from the end of the beam.

If reflections at the end and the associated standing waves are not eliminated, then the amplitude attenuation is not given by $e^{-k''x}$, but by the expression in the numerator of Eq. (4.48). In that case, the amplitude maxima lie on a curve given by $\left[\cosh 2k''(l-x)+1\right]^{1/2} = \sqrt{2}\cosh k''(l-x)$, while the minima are given by $\sqrt{2}\sinh k''(l-x)$. From these two conditions, one may determine $k''$, and thus $\eta$.

The technique of measuring the level reduction with distance along the beam generally yields acceptably accurate results only for $\eta k'l > 10$. With a good sand termination, the limit may be somewhat lower. On the other hand, the half-value bandwidth method is only good up to about $\eta k'l = 2$, see also Figs. 4.8a and 4.8b. In the range between these two limits, one thus needs to vary the length of the test sample somewhat, in order to be able to use one or the other of these two methods.

#### *4.4.2.4 Other Methods*

The previously described methods for determining the elastic properties of beams vibrating in flexure are not the only possible ones. For example, one may also find the loss factor by measuring the frequency interval between response maxima and minima, the distance between the nodes of standing waves, or the mechanical driving point impedance. However, all of these methods have greater disadvantages than those described in detail above, and thus are useful only in special cases.

For quasi-longitudinal waves and torsional waves, which so far have barely been mentioned, one may also use half-value bandwidth, reverberation time, and spatial amplitude attenuation measurements. It should be noted that for such waves there applies the relation $\eta = D'\lambda/27.2$ instead of Eq. (4.71). The same error estimates apply here as before. Care must be taken in all cases that the correct wave form is excited and measured. Particularly for inhomogeneous beams, it is very difficult to avoid exciting several wave types simultaneously, even if symmetry is carefully maintained. Measurements on quasi-longitudinal and torsional waves are generally used for very lightly damped media because of the very small associated radiation damping and at high frequencies in view of the large associated wavelengths.

### 4.4.3 Measurements on Other than Beam-Like Samples

On samples in the shape of plates, rings, cylinders, and the like, one can carry out measurements of the resonance frequencies, half-value bandwidths, and reverberation times much like on beam-shaped samples. However, evaluation of the results is somewhat more difficult, because simple formulas for the resonance frequencies are available only for circular and simply supported rectangular plates, and for rings. For all other configurations, one must use approximate equations for determining the modulus of elasticity from the resonance frequencies. Equations (4.65) and (4.66) apply to the evaluation of the loss factor from the half-value bandwidth, reverberation time, or decay constant, for test samples of any shape. Because the resonance frequencies of plate or shell samples are more closely spaced than those of beams, and are often distributed rather irregularly, one must take particular care to ascertain whether the interval between resonances is greater than the half-value bandwidth. Cylinders and long narrow plates, for example, exhibit a kind of band structure with clusters of resonance frequencies. The complicated distribution of the nodal lines, also often makes it difficult to find appropriate measurement points.

Curved test samples involve additional difficulties, because some of their modes may be much more strongly damped than others. In cylinders, waves which propagate in the axial direction tend to be less strongly damped than circumferential ones. For such samples one must either undertake the tedious process of determining all resonance frequencies and studying the frequency variation of the loss factor in full detail, or one may obtain a general view of the behaviour of the loss factor by exciting the test sample with third-octave or octave band noise and determining the reverberation times in these bands. The latter technique, which is analogous to reverberation measurements in room acoustics, is particularly well suited for samples with very many resonances. It is also useful for cases where there exists strong coupling between the various wave types, due to inhomogeneties and the like.

Yet another possibility relies upon measurements of the input power to the specimen and its spatial average velocity. This implies the determination of force $F(t)$ and velocity $v(t)$ to magnitude and phase at the point of excitation. The product $F(t) \cdot v(t)$ e.g., determined from the cross-spectral densities, represents the power fed to the object and thus the dissipated power under stationary conditions. With a test sample mass $m$, the energy is $E = 1/2\, m < |v|^2 >$, assuming a resonant response. For not too large damping, this energy approximates the reversible energy and Eq. (4.22) can be used to estimate the loss factor as

$$\eta = \frac{E_{diss}}{2\pi E_R} = \frac{W_{diss} T}{\pi m < |v|^2 >} = \frac{2W_{diss}}{\omega m < |v|^2 >} . \qquad (4.71a)$$

## 4.5 Experimental Data

In the literature, material damping is characterized by several different parameters. The relations among the most important damping parameters are given in Table 4.2, in order to facilitate conversion from one to another. Most of these equations apply only for $\eta < 1$.

**Table 4.3.** Mechanical properties of metals at 20°C

| Material | Density kg/m³ | Modulus of Elasticity N/m² | Shear Modulus N/m² | Poisson's Ratio | $c_{LII}$ m/s | $c_T$ m/s | Loss Factor | | Remarks |
|---|---|---|---|---|---|---|---|---|---|
| | | | | | | | Flexural | Longitudinal | |
| Aluminium | 2700 | $72 \cdot 10^9$ | $27 \cdot 10^9$ | 0.34 | 5200 | 3100 | $0.3–10 \cdot 10^{-5}$ | $\approx 10^{-4}$ | [4.19, 20, 24] |
| Lead | 11300 | $17 \cdot 10^9$ | $6 \cdot 10^9$ | 0.43 | 1250 | 730 | $5–30 \cdot 10^{-2}$<br>$1–4 \cdot 10^{-3}$ | $\approx 2 \cdot 10^{-2}$ | [4.19] chem. pure<br>[4.19] Antimon |
| Iron | 7800 | $200 \cdot 10^9$ | $77 \cdot 10^9$ | 0.30 | 5050 | 3100 | $1–4 \cdot 10^{-4}$ | $2–6 \cdot 10^{-4}$ | [4.19, 21, 24] |
| Steel | 7800 | $210 \cdot 10^9$ | $77 \cdot 10^9$ | 0.31 | 5100 | 3100 | $0.2–3 \cdot 10^{-4}$ | | |
| Gold | 19300 | $80 \cdot 10^9$ | $28 \cdot 10^9$ | 0.423 | 2000 | 1200 | $\approx 3 \cdot 10^{-4}$ | | [4.23] |
| Copper | 8900 | $125 \cdot 10^9$ | $46 \cdot 10^9$ | 0.35 | 3700 | 2300 | $2 \cdot 10^{-3}$<br>$2–7 \cdot 10^{-4}$ | $\approx 2 \cdot 10^{-3}$ | Polycrystal<br>single crystal |
| Magnsium | 1740 | $43 \cdot 10^9$ | $17 \cdot 10^9$ | 0.29 | 5000 | 3100 | | $\approx 10^{-4}$ | [4.24] |
| Brass | 8500 | $95 \cdot 10^9$ | $36 \cdot 10^9$ | 0.33 | 3200 | 2100 | $0.2–1 \cdot 10^{-3}$ | $< 10^{-3}$ | [4.19] |
| Nickel | 8900 | $205 \cdot 10^9$ | $77 \cdot 10^9$ | 0.30 | 4800 | 2900 | | $< 10^{-3}$ | [4.24] |
| Silver | 10500 | $80 \cdot 10^9$ | $29 \cdot 10^9$ | 0.37 | 2700 | 1600 | $\approx 4 \cdot 10^{-4}$ | $<3 \cdot 10^{-3}$ | [4.22, 23] |
| Bismuth | 9800 | $3.3 \cdot 10^9$ | $1.3 \cdot 10^9$ | 0.38 | 580 | 360 | | $\approx 8 \cdot 10^{-4}$ | [4.24] |
| Zinc | 7130 | $13.1 \cdot 10^9$ | $5 \cdot 10^9$ | 0.33 | 1350 | 850 | | $\approx 3 \cdot 10^{-4}$ | [4.24] |
| Tin | 7280 | $4.4 \cdot 10^9$ | $1.6 \cdot 10^9$ | 0.39 | 780 | 470 | | $\approx 20 \cdot 10^{-4}$ | [4.24] |

### 4.5.1 Metals

Although the density, modulus of elasticity and Poisson's ratio of metals and thus also the sound speed in metals, are relatively independent of the load history, duration, frequency, etc., that is by no means the case for the loss factor. Numerous and extensive investigations have shown that the interior damping of a metal is strongly affected by relatively small changes in the structure of the metal, such as may be caused by cold rolling, heat treatment and irradiation [4.5, 4.15]. The loss factor of a metal therefore cannot be considered as a material constant. On the contrary, measurements of the loss factor may be used to detect small structural changes. Such measurements are often employed in practice and constitute one ex-

ample of how acoustical measurement techniques may be of great value for metallurgical and solid-state physics investigations. Thus, the loss factor values given in Table 4.3 only provide an indication of the appropriate order of magnitude. (It is an interesting historical fact that very simple measurements on torsionally vibrating wires have long been used to detect fatigue effects) [4.16].

The physical processes that produce the damping of metals are very intricate and not yet fully understood. In addition, it is not at all easy to measure the often very small loss factors, so that some of the values given in the literature do not represent the losses in the material under investigation, but those due to the measurement apparatus (support, excitation system, etc.) or due to sound radiation (particularly for bending waves).

The primary mechanisms responsible for the damping of metals are associated with dislocations in the crystal lattice and with heat conduction between differently strained regions. Investigations concerning dislocation processes [4.16–4.19] are still ongoing, but interpretation of the heat conduction phenomena is relatively well in hand. It merely involves temperature changes produced by strains and the resulting heat conduction and the classical equation of heat conduction and linear thermo-dynamic relations apply.

Upon carrying out the corresponding analysis [4.5] it is found that the damping due to heat conduction appears as a relaxation process. Thereby, the relaxation times are

$$\begin{aligned} \tau &= \left(\lambda / 2\pi\right)^2 C_v \rho / \Lambda, \\ \tau &= \left(h/\pi\right)^2 C_v \rho / \Lambda, \end{aligned} \tag{4.72}$$

for the longitudinal and bending waves respectively. Herein, $C_v$ is the specific heat, $\Lambda$ the thermal conductivity, $\rho$ the density, $\lambda$ longitudinal wavelength and $h$ the plate thickness. With numerical values introduced, where, for most metals $C_v \rho / \Lambda \sim 10^{-3}$, it can be established that some damping occurs at low frequencies for bending waves, typically below 200 Hz, and in the ultrasonic range for longitudinal.. The effect, however, is always small. At the relaxation maximum $\omega\tau = 1$, the loss factor is merely of the order of $10^{-3}$.

The damping process associated with heat conduction is readily interpreted by recognizing that a material is cooled by an extension and heated by a compression. Thus, when the period is too short to allow for a complete equalization of temperature – isothermal case – but too long to realize ideal adiabatic conditions, then there is a small energy remainder which serves to heat the material. The fact that the wavelength appears in Eq. (4.72) on the one hand and the plate thickness on the other, stems from the

distance between elongated and compressed structural regions i.e., cool and hot zones for the two wave types respectively. For the longitudinal wave those zones are typically half a wavelength apart whereas the thickness of the structure separates them in bending.

The damping of bending waves due to heat conduction, has repeatedly been verified experimentally. However, it appears that the measured damping values agree with the theoretical ones only in the vicinity of the relaxation maximum. At higher frequencies, other damping mechanisms (heat conduction between individual crystals, dislocation processes, etc.) tend to predominate. These other mechanisms are responsible for the values given in Table 4.3, obtained under "normal" conditions.

With the exception of lead, tin, silver and copper, the loss factors of metals in general are considerably smaller than $10^{-3}$.

For built-up structures such as machines and vehicles, the differences in the damping of materials are of little importance. The actual damping of such structures is not determined by the losses in the materials, but by friction at supports, interfaces, connections, etc., see Sect. 4.8.

### 4.5.2 Plastics

Because damping measurements have long been used as a tool in investigations of high-polymer materials, and because such materials are very often used as damping treatments, a separate discussion of this group of materials is justified. The mechanical properties of amorphous high polymers characteristically exhibit a very broad transition region between the rigid and the liquid state. In this transition region, the long and possibly cross-linked chains of molecules become increasingly mobile, and there occur relaxation mechanisms which lead to loss factors up to $\eta = 10$. The moduli of elasticity and the loss factors of such materials depend very strongly on temperature and frequency. Thus, complete description of the mechanical properties of such a material involves, for example, curves that show the frequency dependences of these properties at various constant temperatures. An example of such a set of curves, taken from Becker and Oberst [4.24], is shown in Fig. 4.17.

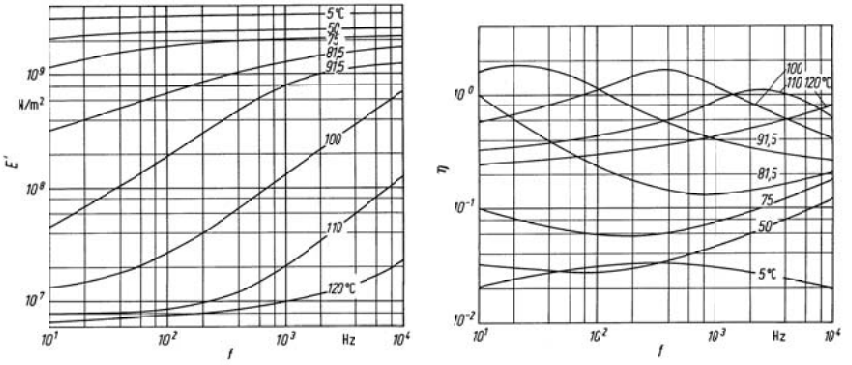


**Fig. 4.17.** Dependence of modulus of elasticity and loss factor of polyvinylchloride on frequency and temperature, [4.24]

Figure 4.17 illustrates the fact that the loss factor is greatest where the modulus of elasticity changes most rapidly with frequency. This sort of behaviour is exactly what one expects for a relaxation process in view of Eqs. (4.4) and (4.5), cf. Fig. 4.2a and Table 4.1. The fact that in reality there are present a multitude of relaxation processes, and not just a single one, does not affect the foregoing considerations.

Several other "laws" apply to amorphous high polymers, in addition to the relation between the loss factor and the frequency dependence of the modulus of elasticity. The most important of these laws are briefly described below.

All plastics have a so-called "freezing" point, below which their properties are much like those of glass. This freezing point or glass-transition temperature is not uniquely defined. It increases with increasing frequency, as evident in Fig. 4.17. Below the glass-transition temperature, most high polymers have a modulus of elasticity of about $5 \cdot 10^9$ N/m$^2$, and a relatively small loss factor, usually less than 0.1. Plastics therefore are not suited for damping applications below their transition temperatures.

Above the glass-transition temperature, there occurs a more or less broad temperature region – the so-called "rubber-elastic" region – in which plastics behave neither entirely like solids, nor like liquids. Because plastics exhibit rather high loss factors in this region, see Table 4.4, it is this region that is best for damping applications. The moduli of elasticity in this transition region are of the order of $10^6$ to $10^7$ N/m$^2$ for "linear" materials that is, for materials with long non-cross-linked molecules. For cross-linked materials, the moduli are of the order of $10^8$ N/m$^2$. The modulus of elasticity of plastics which is of importance for damping layer treatments may be increased somewhat by the addition of fillers e.g., vermiculite. By

**Table 4.4.** Loss factor and modulus of elasticity [N/m$^2$] at maximum damping for some high-polymers

| | | | | |
|---|---|---|---|---|
| Polyvinylchlorid (pure) | $\eta = 1.8$ | $E = 3 \cdot 10^7$ | at 92°C and | 20 Hz |
| Polystyrene | $\eta = 2.0$ | $E = 30 \cdot 10^7$ | at 140°C and | 2000 Hz |
| Polyisobutylene | $\eta = 2.0$ | $E = 0.6 \cdot 10^7$ | at 20°C and | 3000 Hz |
| Nitrile Rubber | $\eta = 0.8$ | $E = 33 \cdot 10^7$ | at 20°C and | 1000 Hz |
| Hard Rubber | $\eta = 1.0$ | $E = 20 \cdot 10^7$ | at 60°C and | 40 Hz |
| Polyvinylchlorid with 30% plasticizer | $\eta = 0.8$ | $E = 2 \cdot 10^7$ | at 50°C and | 100 Hz |

this, materials with loss moduli up to about $E'' = E'\eta = 10^9$ N/m$^2$ can be obtained.

In addition, one may obtain significant changes in the temperature-variations of the properties of plastics by adding "plasticizers". One may thus expect in principle to be able to obtain materials with optimised damping behaviour over prescribed temperature and frequency regions, by using appropriate combinations of cross-linked polymers, fillers, and plasticizers. However, both experience and theoretical considerations [4.25, 4.26] show that the temperature region in which the loss factor is high that is, the "temperature bandwidth" decreases as one increases the maximum loss factor. The variations of the loss factors with frequency behave similarly; the higher the loss factor, the smaller the bandwidth.

But there is more to the relation between the temperature and frequency variations. It was shown, particularly by Williams, Landel and Ferry [4.26], that in the transition region a temperature increase (at constant frequency) corresponds approximately to an increase in the logarithm of the frequency (at constant temperature). Thus, an increase in temperature, a reduction in the frequency, and addition of a plasticizer all have the same qualitative effect. All three changes reduce the modulus of elasticity, and all either increase or decrease the loss factor, depending on where one begins in relation to the position of the loss factor peak.

It should also be pointed out that in most cases the shear modulus is approximately 1/3 of the modulus of elasticity, and that the loss factor in shear differs only negligibly from that in tension and compression.

Beyond the rubber-elastic region, there occurs the plastic, and finally the fluid region. In these regions, any loading results in permanent deformation, and the moduli of elasticity become so small that materials in these regions are neither suitable for structural applications, nor for optimal damping treatments.

### 4.5.3 Building Materials

Other materials, besides metals and plastics, also are important in practice. Table 4.5 lists the moduli of elasticity and loss factors of several such materials in the audio-frequency range. The indicated values are useful only as guidelines, because the mechanical properties of material like concrete, asphalt, brick, etc. are known to depend strongly on their composition and on how they are made.

One may note that the loss factor in very many cases is of the order of $10^{-2}$. Thus, this value may be used as a rough estimate for building structures, as well as for sheet-material structures.

**Table 4.5** Mechanical properties of building materials

| Material | Density kg/m$^3$ | Modulus of elasticity N/m$^2$ | $c_{LII}$ m/s | Loss factor | Remarks |
|---|---|---|---|---|---|
| Asbestos concrete | 2000 | $28 \cdot 10^9$ | $3.7 \cdot 10^3$ | $0.7\text{-}2 \cdot 10^{-2}$ | 23°C, 10% Soft Bituminous content |
| Asphalt | 1800-2300 | $7.7 \cdot 10^9$ | $1.9 \cdot 10^3$ | 0.38 | 13°C, 11% Soft |
| | | $12 \cdot 10^9$ | $2.4 \cdot 10^3$ | 0.21 | Bituminous content |
| | | $21 \cdot 10^9$ | $3.2 \cdot 10^3$ | 0.055 | |
| Oak | 700-1000 | $2\text{-}10 \cdot 10^9$ | $1.5\text{-}3.5 \cdot 10^3$ | $\approx 1 \cdot 10^{-2}$ | 13°C, 8.5% Hard Bituminous content |
| Fiber mats, including matrix and air stiffness | 50-300 | $1.4\text{-}3 \cdot 10^5$ | | $\approx 0.1$ | |
| Fir | 400-700 | $1\text{-}5 \cdot 10^9$ | $\approx 2.5 \cdot 10^3$ | $\approx 8 \cdot 10^{-3}$ | [4.12] |
| Felt | | $0.03 \cdot 10^9$ | | $\approx 6 \cdot 10^{-2}$ | |
| Gypsum board | 1200 | $7 \cdot 10^9$ | $2.4 \cdot 10^3$ | $6 \cdot 10^{-3}$ | [4.32] |
| Glass | 2500 | $60 \cdot 10^9$ | $4.9 \cdot 10^3$ | $0.6\text{-}2 \cdot 10^{-3}$ | [4.32] |
| Pressed-wood panels | 600-700 | $4.6 \cdot 10^9$ | $2.7 \cdot 10^3$ | $1\text{-}3 \cdot 10^{-2}$ | |
| Plaster | 1700 | $4.4 \cdot 10^9$ | $1.6 \cdot 10^3$ | $2\text{-}5 \cdot 10^{-2}$ | |
| Cork | 120-250 | $\approx 0.025 \cdot 10^9$ | $0.43 \cdot 10^3$ | 0.13-0.17 | |
| Light concrete | 1300 | $3.8 \cdot 10^9$ | $1.7 \cdot 10^3$ | $1.5 \cdot 10^{-2}$ | [4.32] |
| Plexiglas | 1150 | $5.6 \cdot 10^9$ | $2.2 \cdot 10^3$ | $2\text{-}4 \cdot 10^{-2}$ | |
| Porous, concrete | 600 | $2 \cdot 10^9$ | $1.7 \cdot 10^3$ | $1 \cdot 10^{-2}$ | [4.32] |
| Sand, dry | $\approx 1500$ | $\approx 0.03 \cdot 10^9$ | $0.1\text{-}0.17 \cdot 10^3$ | 0.06-0.12 | [4.31] |
| Dense concrete | 2300 | $26 \cdot 10^9$ | $3.4 \cdot 10^3$ | $4\text{-}8 \cdot 10^{-3}$ | [4.28. 4.31] |
| Plywood | 600 | $5.4 \cdot 10^9$ | $3 \cdot 10^3$ | $\approx 1.3 \cdot 10^{-2}$ | [4.28. 4.21] |
| Brick | 1900-2200 | $\approx 16 \cdot 10^9$ | $2.5\text{-}3 \cdot 10^3$ | $1\text{-}2 \cdot 10^{-2}$ | [4.28. 4.21] |

## 4.6 Plates with Attached Layers

Whereas previous discussions dealt with more or less homogeneous materials, the discussion to follow deals with very inhomogeneous arrangements. Plates with attached layers, in particular, are of great importance for practical noise control applications. Typical configurations usually consist of a base plate (usually of metal), to which are attached one or more layers of a viscoelastic (e.g., a high-polymer) damping material and possibly additional metal plates. Such systems essentially result in a "division of labour", where the metal plates contribute the necessary strength and the damping material produces desirable structure-borne sound properties.

It is important to note that the loss factors of plates with attached layers may differ greatly for different types of loading. It is therefore important that one knows for which type of loading a given loss factor applies. The case of a plate with a simple attached layer, as discussed in the next section, illustrates how the loss factor for longitudinal waves differs from that for bending waves for such a configuration.

### 4.6.1 Plates with Simple, Extensionally Loaded Layers

A simple means for increasing the damping of metal plates consists of attaching to them a so-called damping layer. The loss factor obtained by this means may be determined simply by referring to the definition in Eq. (4.22). For the case of quasi-longitudinal waves, the reversible mechanical energy is composed of the maximum potential energies in the basic plate and in the attached layer. The total reversible energy, in view of Eq. (3.6), thus is given by

$$W_R = \frac{1}{2}\left(E_1' d_1 + E_2' d_2\right)|\varepsilon|^2 = \frac{1}{2}\left(E_1' d_1 + E_2' d_2\right)\left|\frac{d\xi}{dx}\right|^2, \tag{4.73}$$

where $\xi$ represents the maximum displacement during a period, $E_1'$ and $d_1$ represent the real part of the modulus of elasticity and the thickness of the basic plate, and $E_2'$ and $d_2$ represent these properties of the attached layer. Herein and in the following is considered the energy per unit area and to avoid confusion, $W$ is introduced.

If the losses of the base plate are negligible, then, in view of Eq. (4.21), the energy transformed into heat per cycle of vibration may be found to obey

$$W_{diss} = \pi \eta_2 E_2' d_2 \left|\frac{d\xi}{dx}\right|^2. \tag{4.73a}$$

Thus, the loss factor $\eta_L$ for longitudinal loading is given by

$$\eta_L = \frac{W_{diss}}{2\pi W_R} = \eta_2 \frac{E_2' d_2}{E_1' d_1 + E_2' d_2}. \tag{4.74}$$

As one may note, this loss factor is proportional to the loss modulus $\eta_2 E_2'$. For the best material known so far, this quantity has a value of about $10^9$ N/m$^2$. For sheet steel with $E_1 = 2 \cdot 10^{11}$ N/m$^2$, one finds that for $d_1 = d_2$ the loss factor amounts only to $\eta_L \approx 5 \cdot 10^{-3}$. Thus, quasi-longitudinal waves are very difficult to damp, unless they can be converted into other types of waves.

In the case of bending waves, which is considerably more important for sound radiation, the attached layer also deforms primarily in extension, as shown in Fig. 4.18. If $\xi_M$ represents a displacement at the centre line of the attached layer, then the energy per unit area transformed into heat in one cycle is given by

$$W_{diss} = \pi \eta_2 E_2' d_2 \left| \frac{d\xi_M}{dx} \right|^2. \tag{4.75}$$

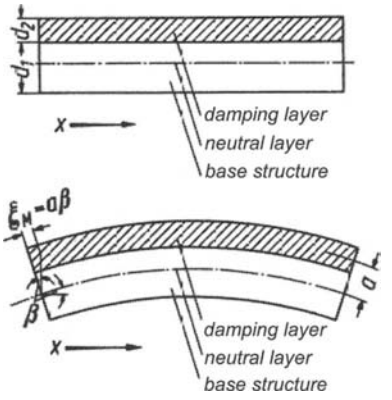


**Fig. 4.18.** Flexure of beam with viscoelastic layer

The reversible mechanical energy in bending, according to Eq. (3.92b), may be expressed as

$$W_R = \frac{1}{2} B \left| \frac{d^2\eta}{dx^2} \right|^2 = \frac{1}{2} B \left| \frac{\partial \beta}{\partial x} \right|^2, \tag{4.75a}$$

where $B$ represents the bending stiffness of the combined system consisting of the plate and the attached layer, and $\beta$ represents the angle of flexure. If $a$ denotes the distance from the neutral fiber to the centre-line of the attached layer, then $\xi_M = a\beta$. Thus, the loss factor $\eta_B$ for bending waves obeys

$$\eta_B = \frac{W_{diss}}{2\pi W_R} = \eta_2 \frac{E_2' d_2 a^2}{B}. \tag{4.76}$$

This expression contains the two quantities, $a$ and $B$, that must still be evaluated. As an approximation [4.33] one may take $a = (d_1 + d_2)/2$, that is, one may assume $a$ to be approximately equal to the distance from the middle of the basic plate to the middle of the attached layer, cf. Sect. 4.6.3.1. One may approximate $B$ as

$$B \approx \frac{E_1 d_1^3}{12} + E_2 d_2 a^2, \tag{4.76a}$$

where the second term is of importance only for relatively thick attached layer ($d_2 > d_1$).

Figure 4.19 shows the dependence of the loss factor ratio $\eta_B/\eta_2$ on the thickness ratio, based on the exact analysis of Oberst [4.12]. Also shown in this figure are points for $E_2'/E_1 = 3\cdot10^{-3}$. Clearly, Eq. (4.76) is a very good approximation.

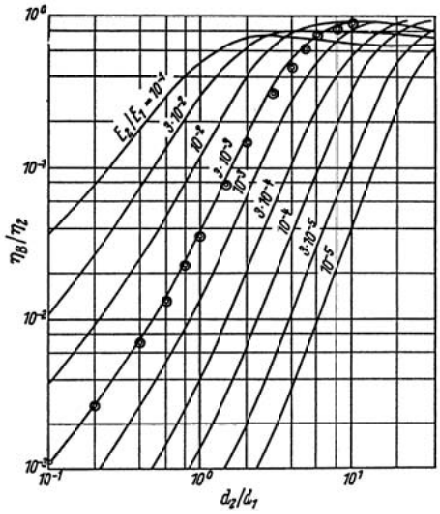


**Fig. 4.19.** Loss factor of beams or plates with single visco-elastic layer, after Oberst. Points show values calculated from the approximate relations, Eqs. (78) and (78a) $E_2'/E_1 = 3\cdot10^{-3}$.

It is interesting to note that the loss factor for bending waves is independent of frequency, as it is for longitudinal waves, but that it is considerably higher for bending waves. Whereas for $E_2'\eta_2 = 10^9$ N/m$^2$, $d_1 = d_2$ and $E_1 = 2 \cdot 10^{11}$ N/m$^2$, it was previously found that the longitudinal-wave loss factor is $\eta_L \approx 5 \cdot 10^{-3}$, for the same configuration and materials the loss factor for bending waves turns out to be $\eta_B \approx 5.5 \cdot 10^{-2}$ – thus, more than 10 times greater.

Experimental measurements made on plates with attached layers have been found to be in good agreement with Fig. 4.19. Therefore, these relations may also be used for the design of damping treatments. As one may note, the total damping increases with increasing values of the product $E_2'\eta_2$ and with increasing thickness $d_2$. The damping layer therefore should not only be thick and have a high loss factor, it should also have as high a modulus of elasticity as possible. Soft materials, such as felt or soft rubber, thus are not well suited for structural damping. Useful damping materials generally consist of filled high-polymer plastics, with moduli of elasticity greater than $10^9$ N/m$^2$ and with as high loss factors as possible.

Beside the previously discussed parameters, the separation distance $a$ (see Fig. 4.18) also plays a significant role. Clearly, one should make $a$ as large as possible. One can accomplish this either by increasing the thickness of the attached layer, or by using a "spacer" between the attached layer and the basic plate, Fig. 4.20. That an increase in the thickness of the attached layer increases the separation distance is obvious; the foregoing considerations also imply that one obtains the greatest amount of damping from a given thickness of damping material by applying it to only one side of the basic plate. The aforementioned spacer [4.34] essentially acts so as to amplify the motion of the basic plate, by a lever action. Ideally, the spacer should be an interlayer with a very high shear stiffness. (One typically uses a metal honeycomb structure as a spacer.) Use of a spacer increases the distance $a$ by the thickness of the spacer, and consequently increases the loss factor considerably. If the spacer does not have a very high shear stiffness, then the increase in the loss factor is less.

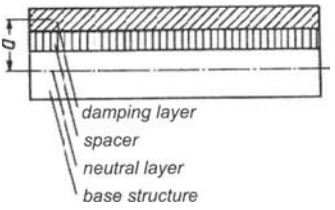


**Fig. 4.20.** Spacing layer for increasing the effect of a visco-elastic layer

### 4.6.2 Plates with Multi-Layer Treatments

It has become common practice to damp plate-like structures by attaching a layer of viscoelastic material and placing atop that layer a secondary "constraining" plate of structural material. Such arrangements are often obtained in practice by use of so-called "damping tape" (a self-adhesive, relatively thick metal foil, where the adhesive is a viscoelastic material) or in sandwich configurations which incorporate an interlayer of a highly dissipative plastic material. Also conceivable are many other "constrained layer" configurations, with or without spacers, see Fig. 4.21. In all of these constrained layer configurations, the viscoelastic material is subjected primarily to shear loading (see Fig. 4.22) caused by the covering plate extending less than the upper surface of the basic plate. The associated displacement difference $\xi_2$ gives rise to the shear angle $\gamma_2 = \xi_2/d_2$. By analogy to Eq. (4.21), one finds that the energy (again per unit area) that is changed into heat within the viscoelastic layer in one cycle is given by

$$W_{diss} = \pi\eta_2 G_2' d_2 \left|\gamma_2\right|^2 = \pi\eta_2 G_2' d_2 \left|\frac{\xi_2}{d_2}\right|^2, \tag{4.77}$$

where $G_2$ represents the shear modulus of the middle layer.

The reversible strain energy here, as previously, is given by

$$W_R = \frac{1}{2} B \left|\frac{d\beta}{dx}\right|^2 = \frac{1}{2} B k^2 \left|\beta\right|^2, \tag{4.78}$$

where $B$ represents the flexural stiffness of the entire composite plate, and is made up of several parts, as will be discussed later.

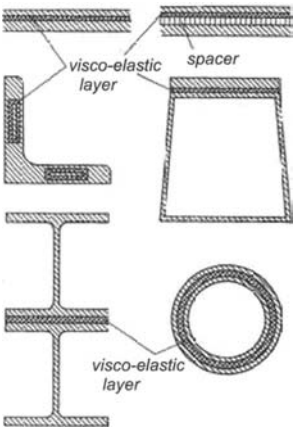


**Fig. 4.21.** Various configurations in which viscoelastic materials act in shear

The $x$-differentiation indicated in Eq. (4.78) may be carried out easily for the case where the entire composite plate vibrates only in flexure, and where the wavelengths of the motions of the two plates and of the interlayer all are the same. For the case of plane waves, from which one may obtain any desired waveform by superposition, the $x$-dependence of all motions is given by $e^{-jkx}$. Here $k = \sqrt[4]{\omega^2 m'/B}$ is the bending wavenumber, which depends on the total mass and total bending stiffness of the composite plate.

The loss factor of a composite plate, in which the energy losses are due primarily to shear of a viscoelastic interlayer, may be found from Eqs. (4.77), (4.78) and (4.22) to be given by

$$\eta = \eta_2 \frac{G_2' d_2 |\gamma_2|^2}{Bk^2 |\beta|^2}. \tag{4.79}$$

This equation still contains two unknown quantities, the flexural stiffness $B$ of the composite plate, and the ratio of the shear angle $\gamma_2$ to the angle of flexure $\beta$. These two quantities are determined below for two special cases. Even without further analysis it is clear that the damping is enlarged by increasing the ratio $\gamma_2/\beta$.

### 4.6.2.1 Stiff Base Plate with Thin Cover Plate

If the damping treatment added to a plate is thin e.g., a damping tape, one may approximate the bending stiffness of the composite by that of the basic plate and take the extension of the viscoelastic layer as $a\beta$, see Fig. 4.22. If one takes into account that the shear forces cause the cover layer to extend by an amount $\xi_3$, then one finds that the shear angle $\gamma_2$ obeys

$$d_2 \gamma_2 = \xi_2 = a\beta - \xi_3. \tag{4.80}$$

One may determine $\xi_3$ from the force $G_2\gamma_2$ that acts on the cover plate and the restoring force in this plate which extends longitudinally. By replacing the inertia force in Eq. (3.3) by the shear force and using Eq. (3.2), one obtains

$$E_3 d_3 \frac{d^2\xi_3}{dx^2} = -\underline{G}_2 \gamma_2, \tag{4.81}$$

where $E_3$ represents the modulus of elasticity of the covering plate.

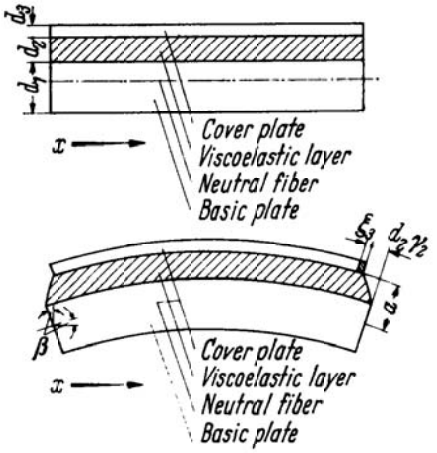


**Fig. 4.22.** Deformation of viscoelastic layer between two plates

Since differentiation with respect to $x$ again is equivalent to multiplication by $k$, one finds from Eqs. (4.80) and (4.81) that

$$\frac{\gamma_2}{\beta} = \frac{a}{d_2} \frac{1}{1 + \dfrac{\underline{G}_2}{E_3 d_3 d_2 k^2}} . \tag{4.82}$$

Note that the complex modulus $\underline{G}_2 = G_2' \left(1 + j\eta_2\right)$ appears above, and not the real part $G_2'$ of the shear modulus, as in Eqs. (4.77) and (4.79). By substituting Eq. (4.82) into (4.79), the loss factor of the composite plate can be written as

$$\eta = \eta_2 \frac{E_3 d_3 a^2 g_d}{B\left|1 + \left(1 + j\eta_2\right) g_d\right|^2}, \tag{4.83}$$

in terms of a so-called "shear parameter" $g_d$ defined as

$$g_d = \frac{G_2'}{E_3 d_3 d_2 k^2} . \tag{4.84}$$

where index $d$ denotes that the covering plate is thin. The shear parameter also may be expressed as

$$g_d = \frac{G_2'}{E_3 d_3 d_2 \omega} \sqrt{\frac{B}{m'}} = \frac{G_2' \lambda^2}{4\pi^2 E_3 d_3 d_2}, \tag{4.84a}$$

where λ represents the bending wavelength of the composite plate. One may note that $g_d$, and therefore also the loss factor of the composite plate, depends on the frequency. In contrast, the loss factor of a plate with a single damping layer was found to be frequency independent. The variation of the loss factor with frequency, as obtained from Eq. (4.83), is shown in Fig. 4.23. As one may observe, there occurs a maximum in the damping. The frequency at which this maximum is obtained is found to obey

$$f_{\max} = \frac{1}{2\pi} \frac{G_2' \sqrt{1+\eta_2^2}}{E_3 d_3 d_2} \sqrt{\frac{B}{m'}} \approx \frac{1}{22} \frac{c_{L1} d_1}{d_2 d_3} \frac{G_2'}{E_3} \sqrt{1+\eta_2^2}, \tag{4.85}$$

where $c_{LI}$ represents the longitudinal wave speed in the base plate.

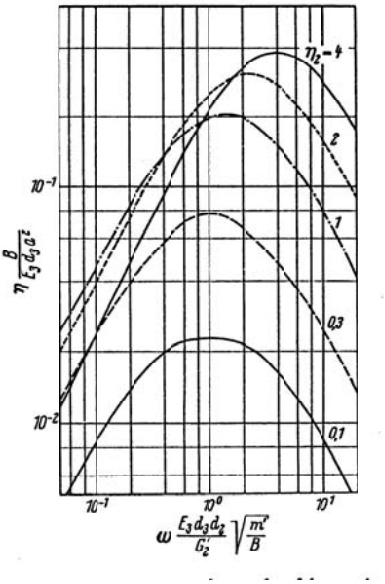


**Fig. 4.23.** Frequency dependence of loss factor of constrained-layer system

Since $c_{LI} \approx 5 \cdot 10^3$ m/sec for metal plates, the shear modulus of the interlayer must be much smaller than the modulus of elasticity of the covering plate, if the frequency corresponding to the damping maximum is to lie in the 100 to 1000 Hz frequency region or primary interest. The decrease in the damping on both sides of the maximum occurs relatively slowly such that the "half-value bandwidth" amounts to about 5 octaves.

There is another important difference between single-layer and multi-layer damping treatments, in addition to the frequency dependence discussed above. Whereas for a single-layer treatment the damping is proportional to the product $\eta_2 E_2'$ (see Eq. (4.76)), the damping of multi-layer treatments does not vary as the product $\eta_2 G_2'$. In fact, Eq. (4.83) indicates that the shear modulus $G_2'$ does not affect the magnitude of the loss factor maximum. $G_2'$ only determines the frequency at which this maximum occurs. In selecting viscoelastic materials here, one thus may primarily ignore the magnitude of $G_2'$, and only choose a material with the largest possible loss factor $\eta_2$. Even relatively soft plastics with $\eta_2 > 1$ may be used effectively, see Table 4.4.

The maximum damping, obtained at the optimum frequency, is given by

$$\eta_{opt} = \frac{E_3 d_3 a^2}{B} \frac{\eta_2}{2\left(1+\sqrt{1+\eta_2^2}\right)}. \tag{4.86}$$

For thick base plates for which $B \approx E_1 d_1^3/12$ and thin covering layers for which $d_1 >> d_2$, $d_1 >> d_3$ and $a \approx d_1/2$, Eq. (4.86) reduces to

$$\eta_{opt} = \frac{3}{2} \frac{E_3 d_3}{E_1 d_1} \frac{\eta_2}{\left(1+\sqrt{1+\eta_2^2}\right)}. \tag{4.86a}$$

The greatest loss factor obtainable with $\eta_2 = 2$ (larger values are extremely rare) is about $0.9\ E_3\ d_3/E_1\ d_1$. By choosing appropriate dimensions, approximately 80 % of this is obtained over a rather wide band of frequencies. The "appropriate dimensions", however, vary for different base plates and must be calculated separately for each special case.

An increase in the temperature results in a decrease in $G_2'$, and thus in a lowering of the frequency at which maximum loss factor occurs.

### *4.6.2.2 Thick Plates with Thin Interlayer*

The formulae derived in the previous section giving a loss factor proportional to $E_3 d_3$ are valid in cases where the top layer is thin and does not notably affect the compound bending stiffness. When this is not the case the formulae must be modified. Since the development is principally the same, reference is made to the literature [4.35]. The problem, moreover, is treated from another aspect in Sect. 4.6.3.2.

For the interpretation it is suitable to introduce a geometry and a shear parameter i.e.,

$$\frac{1}{h} = \frac{B_1 + B_3}{a^2}\left(\frac{1}{E_1 d_1} + \frac{1}{E_3 d_3}\right) \tag{4.87}$$

and

$$g = \frac{G_2'}{d_2 k^2}\left(\frac{1}{E_1 d_1} + \frac{1}{E_3 d_3}\right) \tag{4.87a}$$

respectively, the latter of which is analogous to that in Eq. (4.84). Herein, $B_1$ and $B_3$ are the unassembled bending stiffnesses of the base and top plates respectively and $a \approx d_2 + (d_1 + d_3)/2$ the distance to the neutral layer.

With these parameters, the loss factor of the system reads

$$\eta = \eta_2 \frac{gh}{\left|1 + \left(1 + j\eta_2\right) g\right|^2 + gh\left[g\left(1 + \eta_2^2\right)\right]}. \tag{4.88}$$

Since

$$gh = \frac{G_2'}{d_2 k^2}\frac{a^2}{B_1 + B_3}, \tag{4.88a}$$

the analogy to (4.83) is evident. Similarly, the frequency for damping maximum is obtained by introducing

$$g_{opt} = \frac{1}{\sqrt{1+h}}\frac{1}{\sqrt{1+\eta_2^2}} \tag{4.89}$$

and the maximum by

$$\eta_{opt} = \eta_2 \frac{hg_{opt}}{2\left(1 + g_{opt}\right) + hg_{opt}}. \tag{4.89a}$$

It is readily confirmed that the expressions for a thin top plate are regained for $h << 1$.

For the application of the expressions in (4.88) and (4.89) there is one difficulty, which relates to bending stiffness of the assembled system, required for the bending wavenumber in Eq. (4.87a). Although the complex bending stiffness can be explicitly written as

$$\underline{B} = \left(B_1 + B_3\right)\left(1 + \frac{\underline{g}h}{1 + \underline{g}}\right);\ \underline{g} = g\left(1 + j\eta_2\right), \tag{4.90}$$

the difficulty is not removed since $g$ is required involving $k$, which in turn depends on $B$. It would be possible to calculate $k$ directly (see Sect. 4.6.3)

but this implies high order polynomials and hence an iterative procedure appears easier. This means that $k^2$ is approached by using $B = B_1 + B_3$ or the bending stiffness from $g = g_{opt}$ as the initial value. For the special case of two equal plates i.e., $E_1 = E_3$ and $d_1 = d_3 >> d_2$, the geometry parameter is approximately $h \approx 3$ and thence

$$\eta_{opt} = \eta_2 \frac{3}{5 + 4\sqrt{1+\eta_2^2}} < 0.75 \,. \tag{4.91}$$

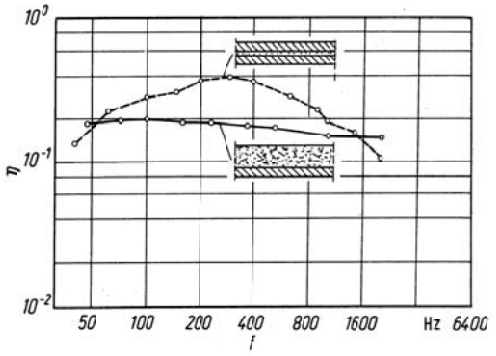


**Fig. 4.24.** Experimentally observed loss factors of a sandwich plate and of a plate with a simple layer ($d_2/d_1 \approx 2.5$)

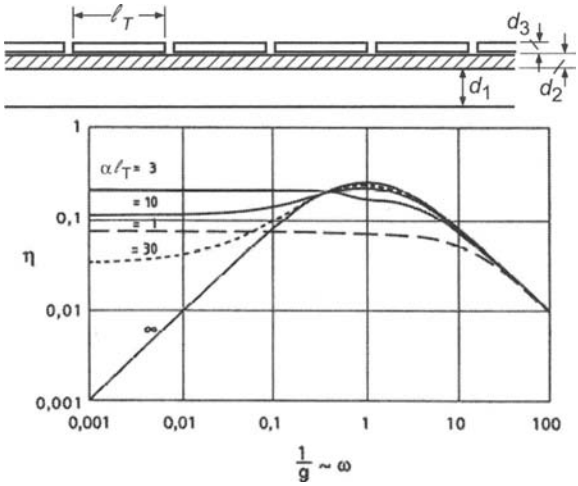


**Fig. 4.25.** Loss factors for a damping layer constrained by a segmented top plate. Parameter $\alpha^2 = \frac{G_2}{d_2}\left(\frac{1}{E_1 d_1} + \frac{1}{E_3 d_3}\right)$

This optimum is attained at a frequency, which is a factor four higher than that given by (4.85).

Measurement results for two plate configurations are shown in Fig. 4.24. Although the three-layer configuration exhibits an increased loss factor for a wide frequency band in comparison with that of the single-sided damped plate, the marked reduction towards low frequencies is often perceived as a disadvantage. Fortunately, this is relatively simply remedied by means of a top plate consisting of short strips. In [4.36, 4.37] is shown that such strips lead to larger shear than the corresponding all-covering top plate and thereby an enhanced low frequency damping. The most suitable strip length is $l_T = 3.3/\alpha$ where $\alpha$ is defined in Fig. 4.25.

In summary, one may thus conclude that three-layer plates are well suited for damping of structure-borne sound when the interlayer is developed for shearing action and the thicknesses and material properties, in particular $G_2$ and $\eta_2$, can be optimised such that the loss factor maximum covers the interesting frequency range. By segmenting the top plate, the performance at low frequencies can be improved.

For equal weight, the loss factors of the three-layer plate and the single-sided damped plate are approximately equal when the best commercially available materials are used in both cases. An interesting advantage of the three-layer configuration is the high bending stiffness at low frequencies, which for equal Young's moduli of the two plates can be approximated by

$$B \approx \frac{1}{12} E_1 \left(d_1 + d_3\right)^3 ; g >> 1. \tag{4.92}$$

For high frequencies, on the other hand, following Eq. (4.90)

$$B \approx B_1 + B_3 = \frac{1}{12} E_1 \left(d_1^3 + d_3^3\right); g << 1. \tag{4.92a}$$

This means that the, for the sound transmission loss pivotal, critical frequency is shifted upwards in frequency [4.38] cf., Chapter 7.

### 4.6.3 Equations of Motion of Layered Plates

#### *4.6.3.1 Free Damping Layers*

For many applications, it is insufficient with only the loss factor derived from static considerations but additional dynamic characteristics must be detailed such as the coupling between flexural and tensional waves. This means that the complete set of the equations of motion must be available.

To achieve this it is suitable to employ Hamilton's principle as was done in Sects. 2.5.1 and 3.8.

Upon assuming that the motions of the two-layer system depicted in Fig. 4.26 can be described by means of the longitudinal motion $\xi_L$ of the plane $y = 0$, the transversal motion $\xi_2$ and a rotation $\beta$, the motion in the $x$-direction $\xi_1$ can be written as

$$\xi_1 = \xi_L + y\beta, \tag{4.93}$$

which is valid for any plane $y$. The actual position of the plane $y = 0$ with respect to the interface between the two layers is not specified. It is arbitrary and need not coincide with the neutral layer. This means, however, that the displacement $\xi_L$ also depends on the choice of the plane $y = 0$, which will be further discussed subsequently.

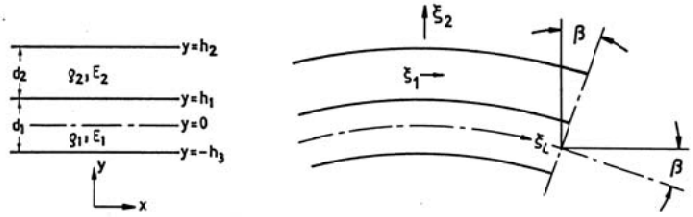


**Fig. 4.26.** Notations for a two-layer system with densities $\rho_1$, $\rho_2$ and Young's moduli $E_1$, $E_2$

For the strain, Eqs. (3.114) to (3.118) yield with the use of (4.93)

$$\begin{aligned} \varepsilon_x &= \frac{\partial \xi_1}{\partial x} = \frac{\partial \xi_L}{\partial x} + y\frac{\partial \beta}{\partial x}, \\ \gamma_{xy} &= \frac{\partial \xi_1}{\partial y} = \frac{\partial \xi_2}{\partial x} = \beta + \frac{\partial \xi_2}{\partial x}. \end{aligned} \tag{4.94}$$

A limitation to Euler-Bernoulli bending theory implies that $\gamma_{xy} = 0$ which gives

$$\beta = -\frac{\partial \xi_2}{\partial x} = -\xi_2'. \tag{4.95}$$

This is the elementary relation between the bending translation and rotation, given in Eq. (3.68) although the sign is changed due to the altered positive direction of the translation. The spatial derivative with respect to $x$

is abbreviated by means of a prime in this section and temporal derivatives by means of a dot.

The approximation in (4.95) could have been omitted for the further analysis. This would have meant that a similar procedure had to be employed as for the treatise of the Timoshenko beam in Sect. 3.8.2. For the sake of brevity, however, this route is discarded since no new information is revealed.

The necessary formulae for the application of Hamilton's principle on a beam of extension $-1 \le x \le 1$ read

$$E_{kin} = \frac{\rho_1}{2}\int_{-1}^{1}\int_{-h_3}^{h_1}\left(\dot{\xi}_1^2 + \dot{\xi}_2^2\right)dxdy + \frac{\rho_2}{2}\int_{-1}^{1}\int_{h_1}^{h_2}\left(\dot{\xi}_1^2 + \dot{\xi}_2^2\right)dxdy\,, \tag{4.96}$$

and

$$\begin{aligned} E_{pot} &= \frac{E_1}{2}\int_{-1}^{1}\int_{-h_3}^{h_1}\varepsilon_x^2\,dxdy + \frac{E_2}{2}\int_{-1}^{1}\int_{h_1}^{h_2}\varepsilon_x^2\,dxdy \\ &= \frac{E_1}{2}\int_{-1}^{1}\int_{-h_3}^{h_1}\left(\xi_L' - y\xi_2''\right)^2 dxdy + \frac{E_2}{2}\int_{-1}^{1}\int_{h_1}^{h_2}\left(\xi_L' - y\xi_2''\right)^2 dxdy. \end{aligned} \tag{4.97}$$

Upon carrying out the integration with respect to $y$, using the abbreviations

$$\begin{aligned} m_E &= \rho_1\int_{-h_3}^{h_1}dy + \rho_2\int_{h_1}^{h_2}dy = \rho_1 d_1 + \rho_2 d_2, \\ m_Z &= \rho_1\int_{-h_3}^{h_1}y\,dy + \rho_2\int_{h_1}^{h_2}y\,dy = \frac{\rho_1}{2}d_1\left(h_1 - h_3\right) + \frac{\rho_2}{2}d_2\left(h_1 + h_2\right), \\ m_D &= \rho_1\int_{-h_3}^{h_1}y^2\,dy + \rho_2\int_{h_1}^{h_2}y^2\,dy \\ &= \frac{\rho_1}{3}d_1\left(h_1^2 - h_1h_3 + h_3^2\right) + \frac{\rho_2}{3}d_2\left(h_1^2 + h_1h_2 + h_2^2\right), \end{aligned} \tag{4.98}$$

and, correspondingly

$$\begin{aligned} E_E &= E_1 d_1 + E_2 d_2, \\ E_Z &= \frac{E_1}{2}d_1\left(h_1 - h_2\right) + \frac{E_2}{2}d_2\left(h_1 + h_2\right), \\ E_D &= \frac{E_1}{3}d_1\left(h_1^2 - h_1h_3 + h_3^2\right) + \frac{E_2}{3}d_2\left(h_1^2 + h_1h_2 + h_2^2\right), \end{aligned} \tag{4.99}$$

one obtains

$$E_{kin} = \frac{1}{2}\int_{-1}^{1}\left(m_E\dot{\xi}_L^2 - 2m_Z\dot{\xi}_L\dot{\xi}_2' + m_D\dot{\xi}_2'^2 + m_E\dot{\xi}_2^2\right)dx,$$
$$E_{pot} = \frac{1}{2}\int_{-1}^{1}\left(E_E\xi_L'^2 - 2E_Z\xi_L'\xi_2'' + E_D\xi_2''^2\right)dx, \tag{4.100}$$

The aim of the following steps is to rewrite the expressions involved in the variation

$$\delta\int_{t_1}^{t_2}\left(E_{kin} - E_{pot}\right)dt$$

so that only $\delta\xi_L$ or $\delta\xi_2$ appear. This is done in accordance with Sect. 3.8 regarding the derivative of the equation of motion for the Timoshenko beam. Again, this is achieved by transferring the derivatives as in Eqs. (3.190f) and (3.190g). In this manner arise linear expressions in $\delta\xi_L$ and $\delta\xi_2$ and those variations can only vanish when the factors in front equal zero i.e.,

$$E_E\xi_L'' - m_E\ddot{\xi}_L - m_Z\ddot{\xi}_2' + E_Z\xi_2''' = 0,$$
$$m_Z\ddot{\xi}_L' - E_Z\xi_L''' - E_D\xi_2'''' - m_E\ddot{\xi}_2 + m_D\ddot{\xi}_2'' = 0 = \left(p_A\right). \tag{4.101}$$

This is thus the equations of motion for a two-layer beam. The pressure $p_A$ is introduced subsequently and represents an externally applied force per unit area (or unit length) acting perpendicular to the plate or beam. It can be incorporated through the variation of the external work $\delta W = p_A\delta\xi_2$ as shown in Eq. (3.188).

As is obvious from a comparison with (3.31) and (3.81), Eq. (4.101) describe the coupling of quasi-longitudinal and flexural waves. $m_E$ is herein the mass per unit area or length, $E_E$ and $E_D$ are the stiffnesses in tension or bending respectively. The coupling comes into play through $E_Z$ and $m_Z$. With the exception of the special case of $E_1/\rho_1 = E_2/\rho_2$, the coupling terms cannot be made to vanish even with a suitable choice of the plane $y = 0$. This means that the bending translation $\xi_2$ is always coupled to a longitudinal motion in a rigorous sense. The coupling, however, can be made very small by making the plane $y = 0$ coincide with the neutral layer of the system, which in this case is given by $E_Z = 0$. From Eq. (4.99) therefore,

$$h_1 = \frac{E_1d_1^2 - E_2d_2^2}{2\left(E_1d_1 + E_2d_2\right)}, \tag{4.102}$$

since $h_3 = d_1 - h_1$ and $h_2 = d_2 + h_1$. The static bending stiffness per unit width of the double-beam thus becomes

$$E_D = B = \frac{E_1 d_1^3}{12} + \frac{E_2 d_2^3}{12} + \frac{E_2 d_2}{1 + E_2 d_2 / E_1 d_1}\left[\left(\frac{d_1 + d_2}{2}\right)^2 - \frac{d_1 d_2}{3}\right]. \tag{4.103}$$

This expression is identical to that used by Oberst [4.12] and almost alike that in Eq. (4.76a). The expression (4.103) can be used to compute the bending wavenumber and the loss factor for complex Young's moduli $E_1$ and $E_2$. The results are identical to those of Sect. 4.6.1 and presented in Fig. 4.19. The same is true for the extensional wave at the neutral layer since, omitting the coupling i.e., with $\omega^2 m_Z = 0$, the wavenumber is given by

$$k_L^2 = \omega^2 \frac{\rho_1 d_1 + \rho_2 d_2}{E_1 d_1 + E_2 d_2}. \tag{4.104}$$

If the principally static consideration is to be avoided wherein $\omega^2 m_Z = 0$, constituting the basis for Eqs. (4.103) and (4.104), the remaining option is to determine the complex wavenumber of the free waves from (4.101). In this pursuit, the wave is assumed in the form $e^{-jkx} e^{j\omega t}$, leading to

$$\begin{aligned} &\left(\omega^2 m_E - k^2 E_E\right)\hat{\xi}_L - jk\left(\omega^2 m_Z + k^2 E_Z\right)\hat{\xi}_2 = 0, \\ &-jk\left(\omega^2 m_Z + k^2 E_Z\right)\hat{\xi}_L + \left(k^4 E_D - \omega^2 m_E - k^2 \omega^2 m_D\right)\hat{\xi}_2 = 0 = \left(p_A\right). \end{aligned} \tag{4.105}$$

The determinant to this system is

$$\begin{aligned} \text{Det} = {} & k^6\left(E_Z^2 - E_E E_D\right) + k^4 \omega^2\left(E_D m_E - 2E_Z m_Z + E_E m_D\right) \\ & + k^2 \omega^2\left[E_E m_E + \omega^2\left(m_Z^2 - m_E m_D\right)\right] - \omega^4 m_E. \end{aligned} \tag{4.106}$$

It is easy to convince oneself that the coefficients of this polynomial are independent of the position of the plane $y = 0$, which is required and initially arbitrarily introduced. If the analysis is confined to the neutral layer i.e., $E_Z = 0$, Eq. (4.106) is simplified but does not split into two equations. To obtain a split, $\omega^2 m_Z$ must be set equal to zero and thus a quasi-static calculation is undertaken. By letting (4.106) equal zero, the solution $\pm k_L$, $\pm k_{BP}$ and $\pm jk_{BN}$ results i.e., the wavenumbers of the extensional and the propagating and evanescent flexural waves. The numerical results are very close to those resulting from a quasi-static analysis.

Equations (4.105), moreover, describe the coupling between the extensional wave motion at the neutral layer $\xi_{LN}$ and the bending motion $\xi_2$. The first equation in (4.105) yields with $E_Z = 0$

$$\frac{\hat{\xi}_{LN}}{\hat{\xi}_2} = \frac{jk\omega^2 m_Z}{\omega^2 m_E - k^2 E_E} \approx -\frac{j\omega^2 m_Z}{kE_E} \approx j\pi \frac{\rho_2 d_2}{\rho_1 d_1} \frac{\lambda\left(d_1 + d_2\right)}{\lambda_{L1}^2}. \tag{4.107}$$

$\lambda_{L1}$ is here the wavelength of the longitudinal wave in beam 1 and $\lambda = 2\pi/k$ the wavelength of the motion of interest e.g., the bending of the system. For the approximation it is assumed that $\lambda_{L1} > \lambda$ and $E_1/\rho_1 > E_2/\rho_2$. It is seen that the coupling between $\xi_2$ and $\xi_{LN}$ indeed exists but that it is weak, particularly at low frequencies since $\lambda < \lambda_{L1}$ as well as $d_1 + d_2 < \lambda_{L1}$. The separate treatment of the two kinds of motion, moreover, is justified by the common applications.

The wave impedance, frequently used in Sect. 4.4, can also be obtained from Eq. (4.105). With $E_Z = 0$,

$$Z_{\sim} = \frac{\hat{p}_A}{\hat{V}_A} = \frac{\hat{p}_A}{j\omega\hat{\xi}_A} = j\omega m_E \left(1 - \frac{k^4 E_D}{\omega^2 m_E} + \frac{k^2 m_D}{m_E} - \frac{k^2\omega^2 m_Z^2}{m_E\left(\omega^2 m_E - k^2 E_E\right)}\right). \tag{4.108}$$

Upon introducing the approximations employed above and letting $k^2 m_D << m_E$, which is also made in ordinary bending theory, one finds

$$\begin{aligned} Z_{\sim} &= j\omega m_E \left(1 - \frac{k^4 E_D}{\omega^2 m_E} + \frac{\omega^2 m_Z^2}{E_E m_E}\right) \\ &\approx j\omega m_E \left[1 - \frac{k^4 E_D}{\omega^2 m_E} + \left\{\frac{\rho_1 d_1}{\rho_2 d_2} \frac{\pi\left(d_1 + d_2\right)}{\lambda_{L1}}\right\}^2\right]. \end{aligned} \tag{4.109}$$

With the exception of the last term within the brackets, this is the wave impedance of an ordinary beam. The correction due to the coupling is again small since $d_1 + d_2 << \lambda_{L1}$.

### *4.6.3.2 Three-layer plates and beams*

The analysis of three-layer systems is similar to that employed for the two-layer structures in the previous section. For the former configuration, however, the shear stiffness plays a profound role and the approximation in (4.95) does not apply. With the notation given in Fig. 4.27, the motions of the three layers read

$$\begin{aligned} \xi_I &= \xi_L + y\beta_I, \\ \xi_{II} &= \xi_L + h_1\beta_I + \left(y - h_1\right)\beta_{II}, \\ \xi_{III} &= \xi_L + h_1\beta_I + d_2\beta_{II} + \left(y - h_1 - d_2\right)\beta_{III}. \end{aligned} \tag{4.110}$$

As before, $\xi_L$ is the displacement in the $x$-direction in the plane $y = 0$, which does not necessarily coincide with the neutral layer. The position of the plane $y = 0$ i.e., the value of $h_1$ is again arbitrary. As in the case of two-layer structures, the displacement $\xi_2$ refers to the $y$-direction. It is the same for all layers in this treatment.

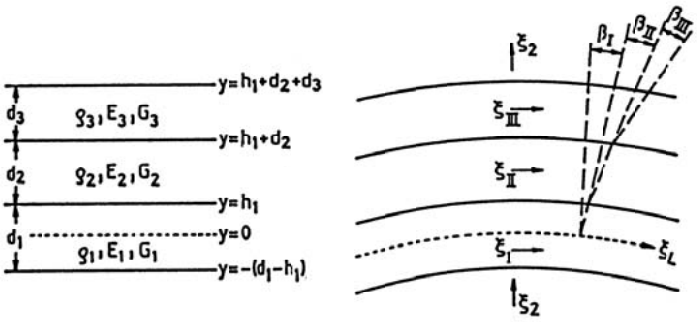


**Fig. 4.27.** Notations for a three-layer system with densities $\rho_1$, $\rho_2$, $\rho_3$, Young's moduli $E_1$, $E_2$, $E_3$ and shear moduli $G_1$, $G_2$, $G_3$

From Eqs. (4.110), the strains become

$$\varepsilon_{Ix} = \frac{\partial \xi_I}{\partial x} = \xi_L' + y\beta_I'; \text{ analogous for } \varepsilon_{II} \text{ and } \varepsilon_{III}$$

$$\gamma_{Ixy} = \frac{\partial \xi_I}{\partial y} + \frac{\partial \xi_2}{\partial x} = \beta_I + \xi_2'; \text{ analogous for } \gamma_{II} \text{ and } \gamma_{III} \tag{4.111}$$

Upon carrying out the same but substantially longer calculation as in the previous section, the equations of motion for the three-layer system result in form of second order differential equations in the variables $\xi_L$, $\xi_2$, $\beta_I$, $\beta_{II}$ and $\beta_{III}$. With the wave motion assumed in the form $e^{-jkx}e^{j\omega t}$, a differentiation with respect to time is a multiplication by $j\omega$ and a differentiation with respect to space a multiplication by $-jk$ and the system of equations can be written as

$$\begin{pmatrix} \alpha_{11} & 0 & \alpha_{13} & \alpha_{14} & \alpha_{15} \\ 0 & \alpha_{22} & \alpha_{23} & \alpha_{24} & \alpha_{25} \\ \alpha_{13} & \alpha_{23} & \alpha_{33} & \alpha_{34} & \alpha_{35} \\ \alpha_{14} & \alpha_{24} & \alpha_{34} & \alpha_{44} & \alpha_{45} \\ \alpha_{15} & \alpha_{25} & \alpha_{35} & \alpha_{45} & \alpha_{55} \end{pmatrix} \begin{pmatrix} \hat{\xi}_L \\ \hat{\xi}_2 \\ \hat{\beta}_I \\ \hat{\beta}_{II} \\ \hat{\beta}_{III} \end{pmatrix} = \begin{pmatrix} 0 \\ p_A \\ 0 \\ 0 \\ 0 \end{pmatrix}, \tag{4.112}$$

when the system is excited by the pressure $p_A$ in the $y$-direction. For a beam-like system, the coefficients are given by:

$$\alpha_{11} = k^2 E_E - \omega^2 m_E \,,\ \alpha_{13} = \left( E_E h_1 - \frac{1}{2} E_1 d_1^2 \right) k^2 - \left( m_E h_1 - \frac{1}{2} \rho_1 d_1^2 \right) \omega^2,$$

$$\alpha_{14} = \left( \frac{1}{2} E_2 d_2^2 + E_3 d_2 d_3 \right) k^2 - \left( \frac{1}{2} \rho_2 d_2^2 + \rho_3 d_2 d_3 \right) \omega^2,$$

$$\alpha_{15} = \frac{1}{2} E_3 d_3^2 k^2 - \frac{1}{2} \rho_3 d_3^2 \omega^2 \,,\ \alpha_{22} = -G_2 k^2 + \omega^2 m_E,$$

$$\alpha_{23} = -jkG_1 d_1, \alpha_{24} = -jkG_2 d_2 \,,\ \alpha_{25} = -jkG_3 d_3,$$

$$\alpha_{33} = \left[ E_E h_1^2 - E_1 d_1^2 \left( h_1 - d_1 / 3 \right) \right] k^2 - \left[ m_E h_1^2 - \rho_1 d_1^2 \left( h_1 - d_1 / 3 \right) \right] \omega^2 + G_1 d_1,$$

$$\alpha_{34} = \alpha_{14} h_1 \,,\ \alpha_{35} = \alpha_{15} h_1,$$

$$\alpha_{44} = \left( \frac{1}{3} E_2 d_2^3 + E_3 d_2^2 d_3 \right) k^2 - \left( \frac{1}{3} \rho_2 d_2^3 + \rho_3 d_2^2 d_3 \right) \omega^2 + G_2 d_2,$$

$$\alpha_{45} = d_2 \alpha_{15} \,,\ \alpha_{55} = \frac{1}{3} E_3 d_3^3 k^2 - \frac{1}{3} \rho_3 d_3^3 \omega^2 + G_3 d_3,$$

$$E_E = E_1 d_1 + E_2 d_2 + E_3 d_3 \,,\ m_E = \rho_1 d_1 + \rho_2 d_2 + \rho_3 d_3,$$

$$G_E = G_1 d_1 + G_2 d_2 + G_3 d_3.$$

Again, the free wavenumbers are determined by equating the determinant of (4.112) to zero and the loss factors are obtained the same way when the moduli are complex. Since the determinant is a fifth order polynomial in $k^2$, there are five solutions at every frequency of which the quasi-longitudinal and the bending type solutions are propagating. The remaining three solutions represent exponentially decaying near fields (evanescent waves).

The wavenumbers can also be computed in analogy with Eq. (4.108). Thereby, is demonstrated that for an excitation and motion in $y$-direction, the free wavenumbers as well as the wave impedance are independent of the arbitrarily chosen $h_1$.

A marked simplification of (4.112) results when it is assumed that no shear occurs in the top and bottom layers, I and II, as is done in simple bending theory. This means that

$$\beta_{III} = \beta_I = -\xi_2' \Rightarrow \beta_{III} = \beta_I = jk\hat{\xi}_2 \tag{4.113}$$

To maintain symmetry of the system of equations, it is suitable to multiply the third and fifth rows by $jk$ and add them to the second. Thereby is obtained

$$\begin{pmatrix} \alpha_{11} - \dfrac{\alpha_{14}^2}{\alpha_{44}} jk & jk\left(\alpha_{13} + \alpha_{15} - \dfrac{\alpha_{14}\gamma_{23}}{\alpha_{44}}\right) \\ jk\left(\alpha_{13} + \alpha_{15} - \dfrac{\alpha_{14}\gamma_{23}}{\alpha_{44}}\right) & \gamma_{22} + k^2 \dfrac{\gamma_{25}^2}{\alpha_{44}} \end{pmatrix} \begin{pmatrix} \hat{\xi}_L \\ \hat{\xi}_2 \end{pmatrix} = \begin{pmatrix} 0 \\ p_A \end{pmatrix} \tag{4.114}$$

in which

$$\gamma_{22} = -k^2 G_2 d_2 + \omega^2 m_E - k^4 \left[ B_1 + B_3 + E_1 d_1 h_{11}^2 + E_3 d_3 h_{13}^2 + E_2 d_2 h_1^2 \right] + \omega^2 k^2 \left[ M_1 + M_3 + \rho_1 d_1 h_{11}^2 + \rho_3 d_3 h_{13}^2 + \rho_2 d_2 h_1^2 \right],$$

$$\gamma_{23} = -G_2 d_2 + k^2 \left[ E_3 d_2 d_3 h_{13} + \frac{1}{2} E_2 d_2^2 h_1 \right] - \omega^2 \left[ \rho_3 d_2 d_3 h_{13} + \frac{1}{2} \rho_2 d_2^2 h_1 \right],$$

$$h_{11} = h_1 - d_1/2\,, \quad h_{13} = h_1 + d_3/2.$$

The quantities $B_1$, $B_3$, $M_1$ and $M_3$ are the bending stiffnesses and second mass moments of inertia of layers I and III respectively, where the intermediate layer is assumed arbitrarily soft,

$$B_1 = \frac{E_1 d_1^3}{12},\ B_3 = \frac{E_3 d_3^3}{12},\ M_1 = \frac{\rho_1 d_1^3}{12},\ M_3 = \frac{\rho_3 d_3^3}{12}.$$

The determinant of Eq. (4.114) is a fourth order polynomial in $k^2$. Upon equating this to zero, the four solutions obtained correspond to propagating quasi-longitudinal and bending waves and evanescent bending and shear waves.

As in conjunction with Eq. (4.101), one may ask the question whether a suitable choice of $h_1$ leads to a decoupling of the two equations in (4.114). Again, this turns out not to be the case without allowing for a frequency dependent $h_1$.

A highly useful approximation for not too high frequencies [4.39] can be achieved by letting $E_2$ vanish. This means that the intermediate layer is assumed to be very soft in compression. It is assumed, moreover, that all inertia terms except $\omega^2 m_E$ can be neglected i.e., $M_1 = M_3 = 0$ and $\rho_2 = \rho_3 = 0$. Hereby, the two equations in (4.114) can be decoupled by selecting $h_1$ such that

$$\alpha_{13} + \alpha_{15} - \frac{\alpha_{14}\gamma_{23}}{\alpha_{44}} = 0 \,,$$

which can be shown to be equivalent to

$$h_1 = \frac{E_1 d_1^2 \left(1+g_3\right) - E_3 d_3^2 g_3 \left(d_3 + 2d_2\right)}{2\left[E_1 d_1 \left(1+g_3\right) + E_3 d_3 g_3\right]}, \tag{4.115}$$

where $g_3 = G_2/(E_3 d_2 d_3 k^2)$. Equation (4.115) presents the position of the neutral layer of a three-layer beam structure. With the approximations introduced above, Eq. (4.114) yields

$$\begin{aligned} &\left[k^2 E_E - \omega^2 m_E - \frac{E_3 d_3 k^2}{1+g_3}\right]\hat{\xi}_{LNF} = 0 \\ &\left\{\omega^2 m_E - k^4\left[B_1 + B_3 + g_3 \frac{E_1 d_1 E_3 d_3}{E_1 d_1 \left(1+g_3\right) + E_3 d_3 g_3}\left(\frac{d_1}{2} + \frac{d_3}{2} + d_2\right)^2\right]\right\}\hat{\xi}_2 = \hat{p}_A \end{aligned} \tag{4.116}$$

The first of the two equations describes the quasi-longitudinal wave at the neutral layer of the three-layered beam. The second describes the bending wave whereby the expression within brackets corresponds to the bending stiffness in (4.90). Hence, the approximation introduced recover the simplified formulae of Sect. 4.6.2.

It should be pointed out that (4.116) implies the solutions of one second and one third order equation in $k^2$ since also $g_3$ depends on $k^2$. Commonly, an initial value is inserted in $g_3$ and an iterative procedure is used.

## 4.7 Damping by means of Resonant Systems

All of the previously discussed composite plates have a rather broadband effect, as is desirable for practical applications where excitation occurs by noise. However, for narrow frequency band excitation such as by transformers and wheel squeal, it is often useful to tune the damping to the narrow band of interest, thereby sacrificing bandwidth for the sake of obtaining very high damping in the narrow band.

The simplest case of such tuned damping resonators consists of independent spring-mass systems attached to the surface that is to be damped.

Consider a rod along which are attached many independent springs and masses, as shown in Fig. 4.28. If quasi-longitudinal waves propagate along the rod, then each of the springs obeys

$$F' = \underline{s}'\left(\xi_S - \xi_M\right), \tag{4.117}$$

where $F'$ denotes the exciting force, $\xi_S$ and $\xi_M$ represent the displacements of the two ends of the spring, and $s'$ denotes the complex spring stiffness. Since all springs here act in shear, one may write

$$\underline{s'} = \underline{G}_F \frac{b}{l} = G'_F \left(1 + j\eta_F\right) \frac{b}{l}, \tag{4.118}$$

where $G_F$ represents the shear modulus, $\eta_F$ the loss factor of the spring material, $l$ the distance between the beam and each attached mass, and $b$ the width of the spring material.

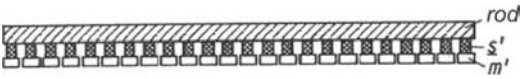


**Fig. 4.28.** Rod with attached damped spring-mass systems

From Newton's law, one finds that the motion of the mass obeys

$$F' = -\omega^2 m' \xi_M, \tag{4.119}$$

where the form of $e^{j\omega t}$ is understood for the motion. If one now introduces the velocity $v_S = j\omega\xi_S$, one obtains

$$F' = \frac{j\omega m' v_S}{1 - \dfrac{\omega^2}{\underline{\omega}_0^2}}, \tag{4.120a}$$

where

$$\underline{\omega}_0^2 = \frac{s'}{m'} = \frac{G'_F b}{l m'} \left(1 + j\eta_F\right) = \omega_0^2 \left(1 + j\eta_F\right) \tag{4.120b}$$

represents the square of the complex natural frequency of each spring-mass system.

In order to determine the vibratory motion, one only needs to apply Eqs. (3.29) and (3.30), after extending these to include the force as given by Eq. (4.120a). The longitudinal motion of a beam with attached springs and masses thus obeys

$$-\frac{dF}{dx} = j\omega\rho S v_S + \frac{j\omega m'}{1-\frac{\omega^2}{\omega_0^2}} v_S,$$
$$-ES\frac{dv_S}{dx} = j\omega F. \tag{4.121}$$

Differentiation with respect to $x$ then leads to

$$\frac{d^2 v_S}{dx^2} + \omega^2 \frac{\rho}{E}\left(1 - \frac{m'}{\rho S}\frac{\omega_0^2\left(1+j\eta_F\right)}{\omega^2 - \omega_0^2 - j\eta_F\omega_0^2}\right) v_S = 0. \tag{4.122}$$

As one would expect, for $m' = 0$ this equation reduces to the usual wave equation.

The attached springs and masses result in changing the wavenumber, which for the original untreated beam is given by $k_{L0}^2 = \omega^2 / c_0^2 = \omega^2 \rho / E$, to the new value $k$, which obeys

$$k^2 = k_{L0}^2\left[1 + \frac{m'}{\rho S}\frac{\left(1-\nu^2\right)+\eta_F^2}{\left(1-\nu^2\right)^2+\eta_F^2} - j\eta_F\frac{m'}{\rho S}\frac{\nu^2}{\left(1-\nu^2\right)^2+\eta_F^2}\right], \tag{4.123}$$

where $\nu = \omega/\omega_0$. This change involves both the real and the imaginary part of the wavenumber. Thus, attachment of the damped springs and masses results in changing both the propagation velocity along the beam and the damping.

Figure 4.29 shows how the propagation velocity and damping vary with frequency, for the case where the attached masses in total amount to 10 % of the mass of the beam. In the vicinity of the resonance, the attached springs and masses may be seen to produce a small change in the propagation velocity and a considerably amount of damping. This damping may even become so high that the assumption of $\eta << 1$ originally made in the derivation does not remain valid.

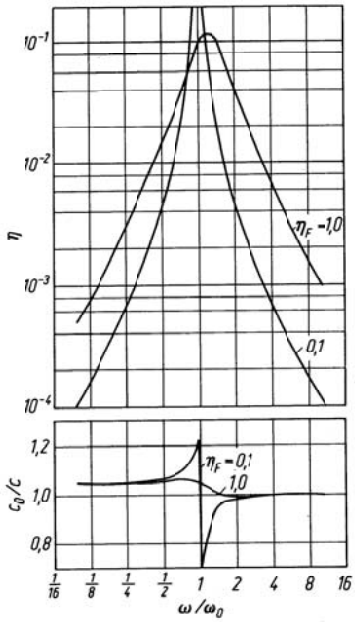


**Fig. 4.29.** Loss factor and propagation velocity of beam with added spring-mass systems, $m'/\rho S = 0.1$

One may readily extend Eqs. (4.117) to (4.123) to other systems attached to the beam, if these systems act independently of each other. One merely needs to use the input impedance

$$\underline{Z'} = \frac{F'}{v_S}$$

of an attached system (per unit length of the beam) in Eq. (4.118) to obtain the differential equation

$$\frac{d^2 v_S}{dx^2} + \omega^2 \frac{\rho}{E}\left(1 - j\frac{\underline{Z'}}{\omega \rho S}\right) v_S = 0, \tag{4.124}$$

which represents a generalization of Eq. (4.122). The real part of the input impedance determines the magnitude of the damping. If this impedance is purely real, the damping can be very large. The driving point impedance of a plate is an example of such a real impedance, see Eq. (4.47). Thus, one may obtain very considerable amounts of damping of quasi-longitudinal

waves by means of thin damped plates attached normal to the axis of the beam. Loss factors of 0.3 are achievable with such configurations.

The damping of the previously discussed systems may also be derived by use of the energy methods of Sect. 4.6. If the loading by the added attached springs and masses is not too great, then the reversible strain energy stored in a beam of length $l$ may be written as

$$W_R'' = \frac{1}{2}\rho S l \left| v_S^2 \right|.$$

The energy lost by the beam per unit time is given by

$$\frac{1}{2} n \operatorname{Re}\{v_S F^*\} = \frac{n}{2} \left| v_S \right|^2 \operatorname{Re}\{\underline{Z}_E\},$$

where $n$ is the number of attached systems and $\underline{Z}_E$ represents the driving point impedance of such systems. Thus, the energy lost per period $T$ of the vibration is

$$W_{diss}'' = \frac{n}{2} \left| v_S \right|^2 T \operatorname{Re}\{\underline{Z}_E\} = \frac{n\pi}{\omega} \left| v_S \right|^2 \operatorname{Re}\{\underline{Z}_E\}.$$

In view of the definition, Eq. (4.22), the loss factor of the total arrangement thus is given by

$$\eta = \frac{n}{l} \frac{\operatorname{Re}\{\underline{Z}_E\}}{\omega \rho S}. \tag{4.125}$$

Since $nZ_E/l$ corresponds to the driving point impedance per unit length, one finds that Eqs. (4.123) and (4.125) give very nearly the same result. The small discrepancy may be ascribed to the fact that the attached systems also store reversible energy, which here has been neglected.

The same kind of analysis as was carried out above for quasi-longitudinal wave can also be performed for torsional and flexural waves. For this purpose, the forces due to the external loads are added to the inertia forces. For bending waves is obtained

$$\frac{d^4 v}{d^4 x} - k_{B0}^4 \left( 1 - j \frac{\underline{Z'}}{\omega \rho S} \right) v = 0 \tag{4.126}$$

instead of Eq. (3.108). Here $\underline{Z'}$ represents the driving-point impedance per unit length of the added system, $\rho S$ denotes the beam mass per unit length, and $k_{B0}$ is the bending wavenumber of the original untreated beam. Clearly, the damping is again determined by the real part of the impedance. For attached simple spring-mass systems, the damping again exhibits a definite peak, and the overall behaviour is much like that indicated in Fig. 4.29.

An example of experimental results for a beam damped by attached resonators is shown in Fig. 4.30 [4.40]. The beam vibrates in flexure and has many small differently tuned sheet-metal strips attached to it, each strip being lightly damped. Nevertheless, this configuration leads to loss factors of 0.01 to 0.02. Although this value is not particularly high (the weight of the added strips was about 9 % of the weight of the beam; for the same amount of added weight one could obtain three to four times as high a loss factor by use of a simple added viscoelastic layer), this type of configuration is likely to be of practical interest for special-purpose applications, because one may obtain almost any desired frequency dependence.

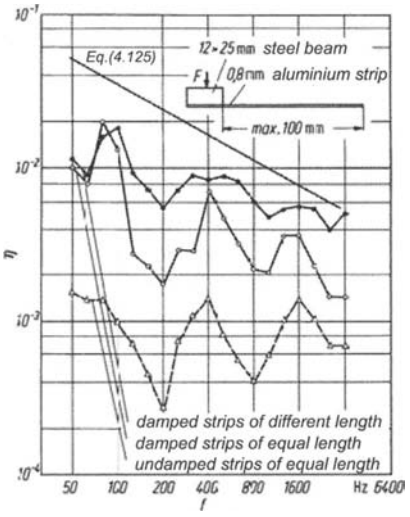


**Fig. 4.30.** Loss factor of beam with sheet-metal strip resonators

Another system in which the damping is of a resonant nature consists of two plates that are interconnected by resilient elements. Such plates in effect are two coupled systems, which may be described by means of two coupled bending-wave equations. The exact expressions obtained for the two bending wavenumbers are rather complicated the general case, see Sect. 6.7.1. However, it is found that the damping is greatest at

$$\omega = \omega_0 = \sqrt{\frac{s''\left(m_1'' + m_2''\right)}{m_1''\, m_2''}},$$

where $s''$ represents the spring-constant of the interlayer per unit area, and $m_1''$ and $m_2''$ denote the masses per unit area of the two plates. $\omega_0$ then represents the resonance frequency of the two masses interconnected by the spring. Above and below $\omega_0$ the damping is relatively small. This fact is sometimes of importance for multi-layer plates with very soft or thick interlayers, for which the relatively high loss factors indicated in Sect. 4.6.2 is not obtained above $\omega_0$. One therefore should be careful not to make the interlayers of multi-layer composites too soft.

### 4.7.1 Damping by Thick Layers (Ballast)

For thick layers, damping is achieved by radiation of structure-borne sound energy to a material with high losses. There is thus a certain resemblance to airborne sound radiation treated in Chapter 7. For the following it is assumed that the wavelength $\lambda_p$ of the vibrating structure is larger than that of the thick lossy layer $c_M/f$. With the quantities of Chapter 7, this means that the radiation efficiency is approximately unity, $\sigma \approx 1$. This approximation implies that the layer can be treated as a one-dimensional wave-guide of density $\rho_M$ and the complex speed of sound $\underline{c}_M$. When the wave-guide is free at the remote end at the distance $d$ from the interface with the structure as depicted in Fig. 4.31, then the input impedance per unit area is

$$\underline{Z}' = j\rho_M \underline{c}_M \tan\left(\omega d / \underline{c}_M\right); \underline{c}_M = c_M' \sqrt{1 + j\eta_M} \tag{4.128}$$

Herein, $\eta_M$ is the loss factor of the layer material. If the base structure performs bending vibrations, $c_M$ is given by the longitudinal wave speed of the layer whereas for longitudinal vibrations, the shear wave speed is to be chosen.

Upon substituting Eq. (4.128) into (4.124) or (4.126), the loss factor of the assembly can be estimated approximately. An example is shown in Fig. 4.31 where extensional waves in an aluminium rod are damped. For the damping is employed a soft rubber layer for which $c_M \approx 100$ m/s and $\eta_M \approx 0.9$. The first thickness resonance of the layer is at about 2000 Hz, $\omega d/c_M = \pi/2$. As can be observed, the loss factor diminishes rapidly below this frequency since only little energy is transmitted to the layer. Above the first thickness resonance, the subsequent resonances are barely visible owing to the high loss factor. In this frequency range it is possible to set $\mathrm{Re}\left[Z_M'\right] \approx \rho_M c_M'$.

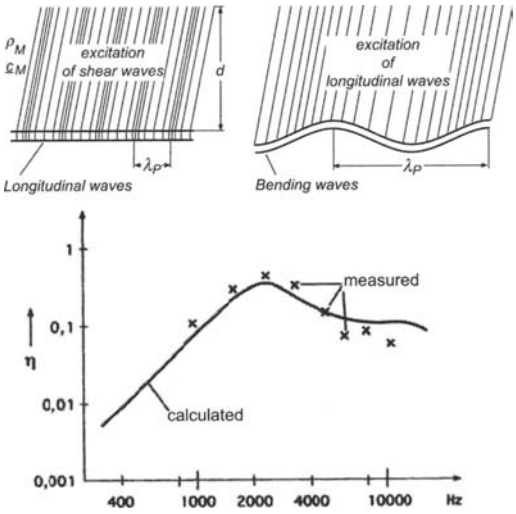


**Fig. 4.31.** Damping by structure borne sound radiation to a thick layer (liner) of soft material ($\lambda_p > c_M/f$)

Compared with a free damping layer treatment of mass equal to that of the thick layer, almost the same loss factor is obtained above the first thickness resonance. Soft, lossy layers accordingly, are suitable for damping of structure-borne sound provided they are sufficiently thick. Their particular advantage is that longitudinal waves are almost as strongly damped as the flexural ones. A drawback is their space consumption; a fact that possibly can be compensated by simultaneous use as airborne sound absorbers.

In [4.41] also, those loss factors are calculated, which are obtained under consideration of the lateral coupling in the liner. In these calculations the continuum expressions are employed i.e., longitudinal and transversal motions of the liner are taken into account. A comparison of the results with those obtained using Eq. (4.128) in (4.124) or (4.126), exhibits hardly any difference. It can be shown that this is always the case whenever $c_M$ is smaller than the governing wave speed of the base structure, the latter of which, for instance, being the bending wave speed.

The treatment of thick layers also encompasses embedding the structure or part there of in sand. Such a solution has the advantages of being cheap and temperature robust. Also in such a case, there is a significant effect at and above the first thickness resonance and the mean of the damping is set by $\mathrm{Re}[Z'_M] \approx \rho_M c'_M$ . Here, $\rho_M$ is the density of sand and $c_M$ is the appropriate wave speed, which can only be quantified with difficulty. It is sug-

gested, however, that for thin, dry, uncompacted sand layers, $c_L \approx 150$ m/s, $c_T \approx 100$ m/s and $\eta \approx 0.1$ [4.42]. These values represent the most favourable case since sand is most often humid. Besides this, the sand is inevitably compacted through gravity and by being vibrated. Both effects therefore, lead to higher wave speed and thence less damping for low and intermediate frequencies. Nevertheless, commercially available dried sand remains an appreciable damping material for intermediate and high frequencies.

## 4.8 Damping at Joints

It is well-known that machines and technical appliances consisting of several structural parts exhibit substantially larger losses than those of the constitutive materials. As an example, the loss factor of a building is almost always about $2 \cdot 10^{-2}$ whereas systems made of steel or aluminium having a material loss factor less than $10^{-3}$, show

$$\eta \approx 5 \cdot 10^{-3}; \; f < 500\text{Hz}$$
$$\eta \approx 2 \cdot 10^{-3}; \; f > 1000\text{Hz}$$

in systems consisting of few, thick substructures such as a ship's hull,

$$\eta \approx 10^{-2}$$

for systems consisting of several, thick or thin parts such as a car body and

$$\eta \approx 5 \cdot 10^{-2}; \; f < 500\text{Hz}$$
$$\eta \approx 10^{-2} \quad ; \; f > 1000\text{Hz}$$

for systems of several thin substructures.

Such "built-in" loss factors are the reason for lower resonant response than would be expected based on only material dissipation. They are also the reason for why damping treatments such as free damping layers, only lead to audible improvements when the loss factor of the assembly is elevated to more than $10^{-2}$.

The added damping observed for built-up systems stems from the small relative motions, at interfaces between subsystems e.g., bolted or riveted joints, typically smaller than $10^{-6}$ m for intermediate and high frequencies. There, the thin interlayers (air, oil, dust) or contacting peaks of the surface roughnesses act as damped miniature springs or dampers. They come into play for relative motions normal or tangential to the contact surface respectively.

### 4.8.1 Damping by Relative Motion Normal to the Interface

Rather comprehensively investigated is the damping due to relative motion normal to an interface with a fluid film (gas pumping or squeeze film damping) [4.43-4.46]. The most essential mechanism behind the energy loss can be understood from calculating the damping of a plate vibrating in a viscous medium with prescribed velocity, see Fig. 4.32. Starting point is the linearized Navier-Stoke's equations for a compressible medium of density $\rho_0$ speed of sound $c_0$ and kinematic viscosity $\nu$ ($\nu_{air} \approx 16 \cdot 10^{-6}$ m$^2$/s, $\nu_{water} \approx 10^{-6}$ m$^2$/s)

$$\begin{aligned}
&\rho_0 \frac{\partial v_x}{\partial t} + \frac{\partial p}{\partial x} - \rho_0 \nu \left( \frac{\partial^2 v_x}{\partial x^2} + \frac{\partial^2 v_x}{\partial y^2} \right) = 0, \\
&\rho_0 \frac{\partial v_y}{\partial t} + \frac{\partial p}{\partial y} - \rho_0 \nu \left( \frac{\partial^2 v_y}{\partial x^2} + \frac{\partial^2 v_y}{\partial y^2} \right) = 0, \\
&\rho_0 \frac{\partial v_x}{\partial x} + \rho_0 \frac{\partial v_y}{\partial y} - \frac{1}{c_0^2} \frac{\partial p}{\partial t} = 0.
\end{aligned} \tag{4.129}$$

Restricting the analysis to harmonic vibrations such that all field variables are in the form $e^{-jk_x x} e^{-jk_y y} e^{j\omega t}$, a set of homogeneous linear equations results from (4.129) by employing the phasor notation. This set of equations has non-trivial solutions as the determinant to the coefficient matrix vanishes i.e., when

$$\begin{aligned}
k_{y1}^2 &= \frac{\omega^2}{c_0^2} \frac{1}{1 + j\omega\nu / c_0^2} - k_x^2 \approx \left( \frac{\omega}{c_0} \right)^2 - k_x^2, \\
k_{y2}^2 &= \frac{-j\omega}{\nu} - k_x^2 \approx \frac{-j\omega}{\nu} \approx \left( \frac{1-j}{\delta} \right)^2.
\end{aligned} \tag{4.129a}$$

The approximations introduced comes about as the kinematic viscosity $\nu$ is small and the thickness of the resulting acoustic boundary layer $\delta = \sqrt{2\nu / \omega}$ usually is of the order of $10^{-4}$m whereas the wavelengths are some orders of magnitude longer. The general solution to Eq. (4.129) for harmonic motion can be written as

$$\begin{aligned}
\hat{v}_x &= \left( A_1 e^{-jk_{y1}y} + A_2 e^{-jk_{y2}y} \right) e^{-jk_x x}, \\
\hat{v}_y &= \left( A_3 e^{-jk_{y1}y} + A_4 e^{-jk_{y2}y} \right) e^{-jk_x x}, \\
\hat{p} &= \left( A_5 e^{-jk_{y1}y} + A_6 e^{-jk_{y2}y} \right) e^{-jk_x x}.
\end{aligned} \tag{4.129b}$$

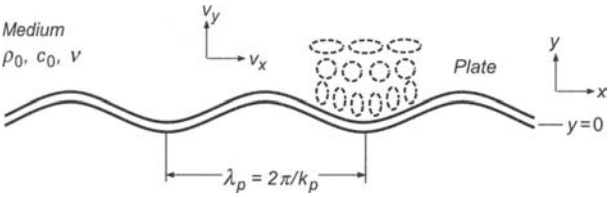


**Fig. 4.32.** Particle motion in a viscous medium adjacent to a vibrating plate

Upon substituting (4.129b) into (4.129), the relations

$$A_3 / A_1 = k_{y1} / k_x,\ A_4 / A_2 = -k_x / k_{y2},$$
$$A_5 / A_1 = \frac{\omega\rho_0}{k_x}\frac{1}{1+j\omega\nu c_0^2},\ A_6 = 0,$$

result for the so far unknown amplitudes. The latter are obtained from the boundary conditions at the plane $y = 0$. In this case, the normal velocity component must equal the plate velocity while the tangential vanishes in a viscous medium i.e.,

$$\hat{v}_y(x,0) = \hat{v}_p e^{-jk_p x},\ \hat{v}_x(x,0) = 0. \tag{4.129c}$$

$k_p = 2\pi/\lambda_p$ is the wavenumber of the plate wave and $\hat{v}_p$ its amplitude. Upon combining the expressions, it is found that

$$\begin{aligned}\hat{v}_y(x,y) &= \frac{\hat{v}_p}{k_{y1}k_{y2}-k_p^2}\left(k_{y1}k_{y2}e^{-jk_{y1}y} - k_p^2 e^{-jk_{y2}y}\right)e^{-jk_p x},\\ \hat{p}(x,y) &= \frac{\hat{v}_p}{1+j\omega\nu/c_0^2}\frac{k_{y2}}{k_{y1}k_{y2}-k_p^2}e^{-jk_{y1}y}e^{-jk_p x},\end{aligned} \tag{4.129d}$$

since $k_x = k_p$. As can be seen, the sound field in front of the plate consists of one part with wavenumber $k_{y1}$ which is of the same order of magnitude as $k_p$ and one part having very large wavenumbers $k_{y2}$. The former part represents either a hydrodynamic nearfield or a propagating wave radiated to the far-field and will be treated in detail in Chapter 7. The latter part is associated with the viscous boundary layer. Usually this boundary layer is neglected because its thickness $\delta$ is so small as was mention above. In the present case, however, it must be taken into account since the small vortices occurring in the layer convert the vibration energy into heat due to the viscosity and act like an energy sink for the plate.

To calculate the damping, it is necessary to develop the power that is transmitted from the plate to the ambient medium. In general the power is given by

$$W = \int \overline{\mathrm{Re}\left[p(x,0,t)\right]\mathrm{Re}\left[v_y(x,0,t)\right]}\,dx = \frac{1}{2}\mathrm{Re}\left[\int \hat{p}(x,0)\,\hat{v}_y^*(x,0)\,dx\right]. \qquad (4.129e)$$

The integration is to be taken over the total length of the plate $l_p$. An averaging over time is indicated by the over bar. Upon substituting the expression in (4.129d) into Eq. (4.129e) is obtained

$$W = \frac{\omega\rho_0 l_p \left|\hat{v}_p\right|^2}{2\left(\frac{\omega^2}{c_0^2} - k_p^2\right)}\left[\mathrm{Re}\left[k_{y1}\right] - \frac{\nu}{\omega}k_p^2\,\mathrm{Im}\left[k_{y2}\right] - \frac{\nu}{\omega}k_p^2\,\frac{\frac{\omega^2}{c_0^2} + k_p^2}{\frac{\omega^2}{c_0^2} - k_p^2}\,\mathrm{Im}\left[k_{y1}\right]\right], \qquad (4.129f)$$

when the small terms $\nu^2\omega^2/c_0^4$ are neglected. Because the wavelength in the plate $\lambda_p$ is substantially larger than the boundary layer thickness $\delta$ in all cases of interest in practice, Im $[k_{y1}]$ << Im $[k_{y2}]$. This means that the first term in (4.129f) representing the radiated sound, and the second, representing the energy conversion to heat, remains whereas the third is insignificant. The loss factor can be obtained by inserting (4.129f) in the definition (4.22) observing that the dissipated energy per period $T$ is given by $E_\nu = W \cdot T = 2\pi W/\omega$. Moreover, approximating the reversible energy by $E_R = \rho h\left|\hat{v}_p\right|^2 \lambda_p / 2$, it follows that

$$\eta = \frac{2W}{\omega\rho h\left|\hat{v}_p\right|^2}. \qquad (4.129g)$$

Herein, $\rho$ is the density of the plate and $h$ its thickness. For thin plates, $|k_{y2}|^2 >> k_p^2 >> \omega^2/c^2$ such that Re $[k_{y1}] \approx 0$ and

$$W \approx \frac{\omega\rho_0 h\left|\hat{v}_p\right|^2 \lambda_p}{4} \Rightarrow \eta \approx \frac{\rho_0\delta}{2\rho h}. \qquad (4.129h)$$

Since the boundary layer thickness $\delta$, as mentioned, is very small and diminishes inversely proportional to the square root of frequency, the loss factor of a system as depicted in Fig. 4.32 is also small and plays a role only for thin folios. Corresponding experiments show that (4.129h) well describes such realizations.

The situation is slightly different for double plates as shown in Fig. 4.33. The previous analysis (4.129a-h), however, applies when account is taken of the fact that for such systems there are also waves in the negative

$y$-direction. This means that terms involving $e^{jk_{y1}y}$ and $e^{jk_{y2}y}$ must be included in (4.129b). With the additional boundary conditions

$$\hat{v}_y(x,0) = \hat{v}_{p1}e^{-jk_{p1}x},\ \hat{v}_y(x,d) = \hat{v}_{p2}e^{-jk_{p2}x},$$
$$\hat{v}_x(x,0) = 0 \qquad ,\hat{v}_x(x,d) = 0,$$

again results a solvable set of linear equations. The explicit analysis is omitted for this case since the outcome is readily understood from Eq. (4.129h).

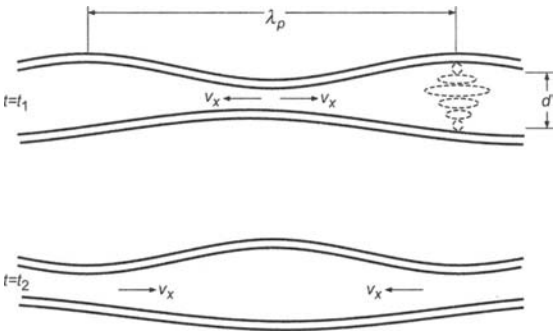


**Fig. 4.33.** Motion at times $t_1$ and $t_2$ for a double plate with a fluid interlayer

As is seen from the previous analysis, the damping is associated with the viscous losses arising by fluid flow in tangential direction. The same is true also for the double plates in Fig. 4.33, the only difference being that the tangential velocity is markedly larger. The reason is that the fluid only has a narrow channel of thickness $d$ in which it can move, implying that the tangential velocity becomes much larger than that in the normal direction. It is readily shown that the flow velocity $v_x$ in tangential direction is a factor $\lambda_p/d$ larger than the normal velocity. Owing to the fact that the dissipated energy is proportional to the velocity squared, it is to be expected that the loss factor $\eta$ of the double plate system is a factor of $(\lambda_p/d)^2$ larger than the value of (4.129h). This is indeed the case since the rigorous treatment [4.44-4.46] reveals a loss factor of

$$\eta \approx \frac{\rho_0 d}{\rho h}\left(\frac{\lambda_p}{2\pi d}\right)^2, \tag{4.130}$$

for a double plate system for which the gas pumping or squeeze film damping is the governing loss mechanism. In Fig. 4.34 is shown, a few ex-

perimental results [4.44] for a case where one plate could be considered rigid. Herein is observed the slope, which is proportional to $f^{-3/2}$ associated with the fact that $\delta$ as well as $\lambda_p$ are inversely proportional to the square root of frequency, exhibited by both experimental and theoretical results. Figure 4.34 also includes two comparative measurements results to demonstrate that the fluid interlayer governs the damping. Squeeze film damping, however, is not the only damping mechanism for thin double plates that exhibit a relative motion in the normal direction but the most important. Other mechanism, besides gas pumping, can be assessed by modelling the interlayer as many small damped springs joining the two plates for which the discussion in conjunction with Eq. (4.127) is valid.

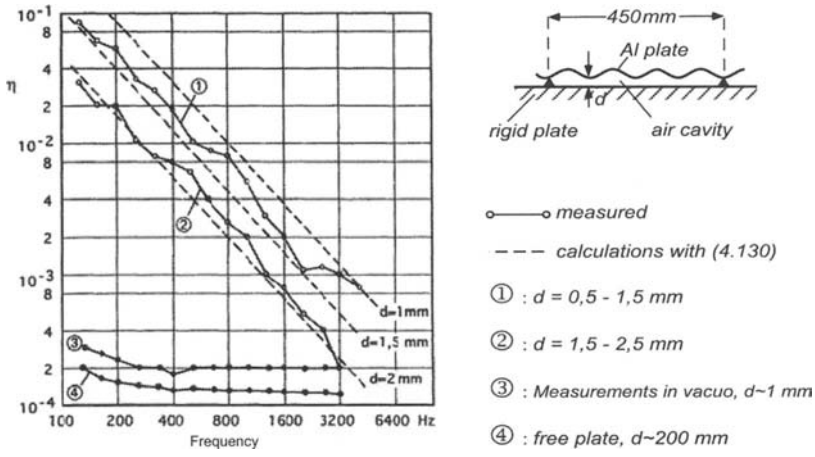


**Fig. 4.34.** Measured and calculated loss factor for a squeeze film damped, 1mm aluminium plate

### 4.8.2 Damping by Relative Motion Tangential to the Interface

For built-up systems consisting of thick substructures such as engines or industrial machines, the motion perpendicular to a junction or interface is usually very small and hence does not lead to significant damping. Instead, the tangential relative motion becomes the governing.

When an interface encompasses a thin viscous film e.g., oil, dust, etc., Sect. 4.6.2 regarding multi-layered systems apply i.e., the interlayer acts in

shear and converts a fraction of the structure-borne sound energy into heat owing to its dissipation. A theoretical assessment of the loss factors is in this case in principle possible for harmonic motion by replacing the viscosity by a complex shear stiffness.

Employing the definitions of the viscosity $\nu = \tau/v$ and the shear modulus $G = \tau/\xi$ and using the relation $\hat{v} = j\omega\hat{\xi}$ for harmonic motion, it is found that

$$\underline{G} = j\omega\nu \,, \tag{4.131a}$$

which is purely imaginary. An introduction of this shear modulus in the expressions of Sect. 4.6.2 therefore implies the following substitution

$$\begin{aligned} &\underline{G}_2 = j\omega\nu_2 \,, G_2'' = \eta_2 G_2' = \omega\nu_2 \,, \\ &\eta_2 g_d = \omega\nu_2 \frac{1}{E_3 d_3 d_2 k^2} \quad , \quad \frac{\omega\nu_2}{d_2 k^2}\left(\frac{1}{E_1 d_1} + \frac{1}{E_3 d_3}\right). \end{aligned} \tag{4.131b}$$

Numerically, one finds that the loss factor is the bigger the smaller the interlayer thickness, $d_2$.

Somewhat more intricate is the situation where dry friction occurs at the interface. Two cases must be distinguished according to the present knowledge.

a) When the amplitudes of the relative motion in tangential direction are not too small but larger than some μm, i.e. above all for low frequencies, the Coulomb friction apply. This means that the process is non-linear since the stick and slip motions follow different laws. The corresponding analysis [4.47-4.49] shows that an increase in amplitude increases the loss factor. It would lead way out of the scope of this book to include the associated analysis.

b) For small motion amplitude, present at intermediate and high frequencies, measurements show only weak amplitude dependence of the loss factor. It thus appears possible to model the interface by many small, damped springs, as illustrated in Fig. 4.35a. The stiffness per unit area for cut steel surfaces is given approximately by the empirical formula [4.50, 4.51]

$$\frac{G_2}{d_2} = 800\left(p_N\right)^{2/3}$$

where $p_N$ is the normal pressure in N/mm$^2$ and the constant such that $G_2/d_2$ has the proper dimension of N/mm$^3$. Some measurement results are shown in Fig. 4.35b. It is expected that the interlayer stiffness increases with increasing normal pressure. The loss factor lies between $10^{-2}$ and $10^{-1}$ and tends to decrease with increasing

normal pressure. With the surface roughnesses commonly found in machine manufacturing, the interlayer stiffnesses and loss factors observed for dry joints between metals are remarkably similar. In measurements of interlayer stiffness and loss factors was observed only a negligible reduction when the average roughness was altered from 5 μm to 40 μm.

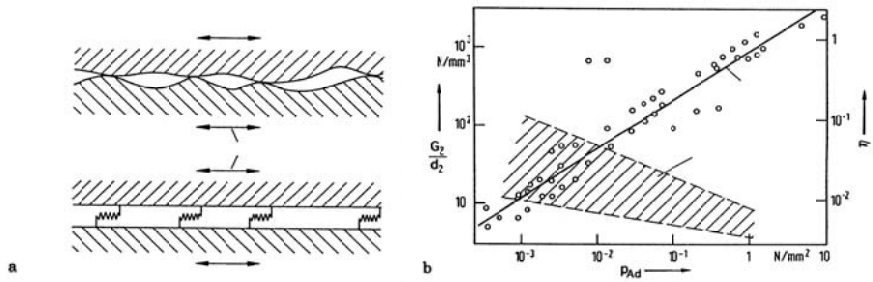


**Fig. 4.35.** Conditions at dry joints with tangential relative motion. (a) Idealized interface and mechanical model. (b) Stiffness and loss factor versus normal pressure

## References

[4.1] Meyer O.E., 1874. Zur Theorie der inneren Reibung. Journal für reine und angewandte Mathematik, 78, p. 130

[4.2] Voigt W., 1892. Über innere Reibung fester Körper, insbesondere der Metalle. Annalen der Physik, 47, p. 671

[4.3] Boltzmann L., 1876. Zur Theorie der elastischen Nachwirkung. Annalen der Physik, Erg. Bd. 7, p. 624

[4.4]Maxwell J.C., 1867. On the dynamical theory of gases. Phil. Trans. Royal Soc., 157, p. 49

[4.5] Zener C., 1948. Elasticity and Anelasticity in Metals. University of Chicago Press, Chicago MI

[4.6] Tamm K. and Weiss O., 1959. Untersuchungen über periodische Wellen, exponentielle und komplexe Nahfelder im begrenzten Festkörper. Acustica, 9, p. 275

[4.7] Weiss O., 1959. Über die Schallausbreitung in verlustbehafteten Medien mit komplexem Schub- und Kompressionsmodul. Acustica, 9, p. 387

[4.8] Cremer L., 1934. Vierpoldarstellung und Resonanzkurven bei schwingenden Stäben. Sitzungsberichte der Preussischen. Akademie der Wissenschaften, phys.-math. Kl. I, p. 1

[4.9] Mason W.P., 1958. Physical acoustics and the properties of solids. Van Nostrand, New York NY

[4.10] DIN 53515: Bestimmung der viskoelastischen Eigenschaften von Gummi. Beuth Vertrieb, Berlin
[4.11] Fitzgerald E.R. and Ferry J.D., 1953. Method for determining the dynamic mechanical behaviour of gels and solids at audio-frequencies–Comparison of mechanical and electrical properties. Journal of Colloid Science, 8, p. 1
[4.12] Oberst H. and Frankenfeld K., 1952. Über die Dämpfung der Biegeschwingungen dünner Bleche durch festhaftende Beläge. Acustica, 2 Beihefte No. 4, p. 181
[4.13] Oberst H., Becker G.W. and Frankenfeld K., 1954. Über die Dämpfung der Biegeschwingungen dünner Bleche durch fest haftende Beläge II. Akustische Beihefte Heft 1 (in Acustica, 4), p. 433
[4.14] Nijman E.J.M. and Bellussi G.N.M., 2000. Helium as good as vacuum: The poor man's approach for accurate material damping measurements. Applied Acoustics, 60, p. 385
[4.15] Truell R. and Elbaum C., 1961. High frequency ultrasonic stress waves. Handbuch der Physik (S. Flügge ed.). Springer Verlag, Berlin
[4.16] Love A.E.H., 1948. A treatise on the mathematical theory of elasticity, p.119. Dover Publications, New York NY
[4.17] Lücke K., 1962. Die von den Kristallbaufehlern und insbesondere von den Versetzungen verursachten Dämpfungserscheinungen. Metallkunde, 53, p. 57
[4.18] Bordoni P.G., 1960. Dislocation relaxation at high frequencies. Nuovo Cimento, Suppl. 1, 17, p. 43
[4.19] Wegel R. and Walter H., 1953. Internal dissipation in solids for small cyclic strains. Physics, 6, p. 141
[4.20] Zemanek Jr. J. and Rudnik I., 1961. Attenuation and dispersion of elastic waves in a cylindrical bar. Journal of the Acoustical Society of America, 33, p. 1283
[4.21] Bennewitz K. and Rötger H., 1936. Über die innere Reibung fester Körper; Absorptionsfrekvenzen von Metallen im akustischen Gebiet. Physikalische Zeitschrift, 37, p. 578
[4.22] Bordoni P.G., Nuovo M. and Verdini L., 1959. Relaxation of dislocations in cubic face-cantered metals. Proc. 3rd International Congress on Acoustics, Stuttgart, Vol. 1, p. 583. Elsevier, Amsterdam (1961)
[4.23] Förster F. and Köster W., 1937. Elastizitätsmodul und Dämpfung in Abhängigkeit vom Werkstoffzustand. Metallkunde, 29, p. 116.
[4.24] Becker G.W. and Oberst H., 1956. Über das dynamisch-elastische Verhalten linear, vernetzter und gefüllter Kunststoffe. Kolloid Zeitschrift, 148, p. 6
[4.25] Linhardt F. and Oberst H., 1961. Über dieTemperaturabhängigkeit schwingungsdämpfender Kunststoffe. Acustica, 11, p. 255
[4.26] Williams M.L., Landel R.F. and Ferry J.D., 1955. Mechanical properties of substances of high molecular weight .19. The temperature dependence of relaxation mechanisms in amorphous polymers and other glass-forming liquids. Journal of the American Chemical Society, 77, p.3701
[4.27] Watters B.G., 1959. Transmission loss of some masonry walls. Journal of the Acoustical Societyt of America, 31, p. 898

[4.28] Kuhl W. and Kaiser H., 1952. Absorption of structure-borne sound in building materials without and with sand-filled cavities. Acustica, 2, p. 179
[4.29] Heckl M. and Nutsch J., 1995. Taschenbuch der Technischen Akustik, 2nd ed., Ch. 22 (M. Heckl, H.A. Müller eds.). Springer Verlag, Berlin
[4.30] Kurtze G., 1956. Körperschalldämpfung durch körnige Medien. VDI-Berichte 8, p. 110
[4.31] Kirstein T. and Müller H.W., 1960. Berichte des Beirats für Bauforschung beim Bundesminister für Wohnungsbau, H 13, Körperschall in Gebäuden. Ernst & Sohn, Berlin
[4.32] Cremer L., 1963. Akustische Versuche an schwimmend verlegten Asphaltestrichen. Bitumen, 25, p. 93
[4.33] Kerwin Jr. E.M., 1959. Damping of flexural waves by a constrained viscoelastic layer. Journal of the Acoustical Societyt of America, 31, p. 952
[4.34] Kerwin Jr. E.M., 1959. Damping of flexural waves in plates by spaced damping treatments having spacers of finite stiffness. Proc. 3rd International Congress on Acoustics, Stuttgart, Vol. 1, p. 412. Elsevier, Amsterdam (1961)
[4.35] Ross D., Ungar E.E. and Kerwin E.M., 1962. Structural damping. American Society of Mechanical Engineeing, New York NY
[4.36] Parfitt G.G., 1962. The effect of cuts in damping tapes. Proc. 4th International Congress on Acoustics, Copenhagen, Paper P 21
[4.37] Zeinetdinova R.Z., Naumkina N.I. and Tartakowski B.D., 1978. Effectiveness of a vibration-absorbing coating with a cut constraining layer. Soviet Physics Acoustics, 24, p. 347
[4.38] Kurtze G. and Watters B.G., 1959. New wall design for high transmission loss or high damping. Journal of the Acoustical Society of America, 31, p. 739
[4.39] Mead D.J. and Markus S., 1985. Coupled flexural, longitudinal and shear wave motion in two- or three-layered damped beams. Journal of Sound and Vibration, 99, p. 501
[4.40] Heckl M., 1961. Wave propagation on beam-plate systems. Journal of the Acoustical Society of America, 33, p. 640
[4.41] Albrecht A. and Möser M., 1989. Die dämpfende Wirkung dicker Entdröhnschichten auf Platten. Zeitschrift für Lärmbekämpfung, 36, p. 73
[4.42] Schmidt H., 1954. Die Schallausbreitung in körnigen Substanzen. Acustica, 4, p. 639
[4.43] Maidanik G., 1966. Energy dissipation associated with gas-pumping in structural joints. Journal of the Acoustical Society of America, 40, p. 1064
[4.44] Trochidis A., 1982. Körperschalldämpfung mittels Gas- oder Flüssigkeitsschichten. Acustica, 51, p. 201
[4.45] Chow L.C. and Pinnington R.J., 1987. Practical industrial method of increasing structural damping in machinery, I: Squeeze-film damping with air. Journal of Sound and Vibration, 118, p. 123
[4.46] Chow L.C. and Pinnington R.J., 1987. Practical industrial method of increasing structural damping in machinery, II: Squeeze-film damping with air. Journal of Sound and Vibration, 118, p. 333

[4.47] Ott D., 1978. Untersuchungen zur Schwingungsdämpfung durch Hysterese in Schraub- und Nietverbindungen. VDI-Berichte 320
[4.48] Mindlin R.D. and Deresiewicz H., 1953. Elastic spheres in contact under varying oblique forces. Trans. ASME, Journal of Applied Mechanics, 20, p. 327
[4.49] Gaul L., 1981. On the damping and transmission of flexural waves at structural joints. Ingenieur-Archiv, 51, p. 101
[4.50] Petuelli G., 1983. Theoretische und experimentelle Bestimmung der Steifigkeits- und Dämpfungseigenschaften normalbelasteter Fügestellen. Diss. RWTH, Aachen
[4.51] Schober U., 1990. Untersuchungen der Körperschalldämpfung durch Fügestellen in Motoren. Proc. of DAGA, Wien, p. 349